International Journal of Fatigue 102 (2017) 59–78

Contents lists available at ScienceDirect

International Journal of Fatigue

journal homepage: www.elsevier.com/locate/ijfatigue

Continuum damage mechanics based approach to study the effects of the scarf angle, surface friction and clamping force over the fatigue life of scarf bolted joints

Zhixin Zhan [a], Qingchun Meng [a], Weiping Hu [a,*], Ying Sun [a], Fei Shen [b], Yanjun Zhang [c]

[a] School of Aeronautics Science and Engineering, Beihang University, Beijing 100191, China
[b] School of Mechanical and Aerospace Engineering, Nanyang Technological University, Singapore 639798, Singapore
[c] The First Aircraft Institute of AVIC, Xi'an 710089, China

ARTICLE INFO

Article history:
Received 17 January 2017
Received in revised form 19 April 2017
Accepted 22 April 2017
Available online 25 April 2017

Keywords:
Continuum damage mechanics
Fatigue life
Scarf bolted joint
Scarf angle
Clamping force

ABSTRACT

In this study, an approach based on continuum damage mechanics is applied to the fatigue life prediction and to analysing the influence of various factor on scarf bolted joints used in an aircraft fuselage. First, the damage-coupled elastic-plastic constitutive equations and fatigue damage evolution equations are presented, and the corresponding numerical calculation algorithm is established using the ABAQUS platform. Then, the proposed fatigue damage model is validated by a group of fatigue tests on scarf joints. Subsequently, the aforementioned approach is applied to the influencing factor analysis of scarf bolted joints. The effects of the scarf angle, the surface friction and the clamping force are investigated in detail. In addition, the sensitivity of the fatigue life with respect to the scarf angle, surface friction and clamping force is evaluated. The effect mechanisms of these factors are revealed clearly, and the influencing trends are presented quantitatively, which has important practical significance for the design of scarf joints.
© 2017 Elsevier Ltd. All rights reserved.

1. Introduction

In engineering applications, bolted joints are widely used to connect two components together to form an integrated structure. Because of their high reliability, being simple to manufacture and assemble and being easy to disassemble, bolted joints have become one of the most common connection types in aircraft structures [1]. Furthermore, the fatigue behaviour of bolted joints has attracted a number of concerns. These concerns are based on two reasons. According to statistics, the fatigue failure of the bolt hole is one of the most common failure patterns in aircraft structures [2,3]. Conversely, it is difficult to accurately evaluate the fatigue properties of joints due to the complexity of the stress state around the bolt hole and the numerous influencing factors, such as the local stress concentration around the hole [4,5], the manufacturing process, the strengthening technology, the clamping force and the surface friction [6,7].

In recent years, a number of studies have been conducted to analyse the fatigue failure around the bolt holes of joints, and many achievements have been reached. Ralph et al. [8] and Liu et al. [9] studied the effect of the manufacturing process of the hole on the fatigue performance of the joints, and the result showed that the fatigue lives are strongly dependent on the quality of the surface finish. Based on the fatigue experiments of joints, Chakherlou [10,11] studied the effect of the magnitude of the interference and the clamping force on the fatigue life, and the results showed that the interference fit can increase the fatigue life and for a given cyclic longitudinal load, at the beginning stage, the increase of the bolt clamping force improves the fatigue life of the bolted joints, however, the further increase of the bolt clamping force could result in an opposite effect by decreasing the fatigue life of joints due to appearance of the fretting. The research of Lacarac et al. [12] showed that cold extrusion strengthening can effectively prevent crack initiation at a high stress area and can improve the fatigue life of joints. Sun [13,14] investigated the effect of interference, cold expansion, the clamping force and the failure mode on the fatigue properties of bolted joints using a damage mechanics based approach.

Scarf bolted joints, as a typical joint, the weight of which is lighter than that of general lap bolted joints because the two plates are directly connected by bolts instead of being connected using laps. Scarf bolted joints can prolonging the fatigue life of joints by averaging the load bearing ratio of every bolt. However, studies of scarf bolted joints are scarce. Yuan et al. [15] conducted an

* Corresponding author at: Room D604, New Main Building, 37th Xueyuan Road, Beihang University, Beijing 100191, China.
E-mail address: huweiping@buaa.edu.cn (W. Hu).

http://dx.doi.org/10.1016/j.ijfatigue.2017.04.008
0142-1123/© 2017 Elsevier Ltd. All rights reserved.

experimental and analytical investigation of the fatigue and fracture behaviours of scarfed lap riveted joints. However, they did not discuss the impact of the scarf angle, surface friction and clamping force on the fatigue performance of the scarf bolted joints. Therefore, the aim of this study was to investigate the influences of these factors and to evaluate the sensitivity of the fatigue life to these factors.

An appropriate approach to the fatigue life prediction of scarf joints is crucial. In recent decades, some methods have been proposed to predict the fatigue life of bolted joints. The local stress strain method [16,17] is a widely used method, which is based on the local stress strain history and the material fatigue characteristic curve considering the effect of plastic deformation of the materials. The stress severity factor (SSF) [18,19] method uses the concept of the SSF to account for the effects of localized stress concentrations or discontinuities in the structural geometry. The Smith–Watson–Topper (SWT) [20,21] method, which is an effective criterion in plain fatigue problems and searches for the maximum fatigue parameter over a number of planes, can also be adopted to predict fatigue life of bolted joints. However, the results based on these methods essentially depend on the initial stress and the strain field. Actually, the local stress and strain fields are affected by the clamping force, friction coefficient, remote stress and geometry features. Meanwhile, the fields keep changing as the number of cyclic loading increases. Thus, these methods can't investigate the effects of the factors, such as the clamping force, friction coefficient, remote stress, and geometry features in detail, because they do not have the ability to describe the fatigue damage process of the joints before failure. An approach based on continuum damage mechanics (CDM) can describe the evolution of the fatigue damage continuously by introducing a damage variables to represent the damage state of materials and by constructing a damage evolution equation to reflect the developing law of damage [22]. Based on the theory of thermodynamics, damage evolution laws combined with damage-coupled elasto-plastic or visco-plastic constitutive models can be derived to model the damage evolution of ductile, fatigue, creep and creep-fatigue, etc. [23]. As the CDM provides a new method for describing the damage evolution in the material, it has been widely used in practical engineering applications [24–26].

In this study, a CDM based method is proposed to predict the fatigue life of a scarf bolted joint. First, a damage-coupled elastic-plastic constitutive model is adopted to represent the material behaviour, and Lemaitre's elastic and plastic damage evolution equations are applied to calculate damage accumulation. Second, the corresponding damage mechanics, and a finite element numerical simulation is implemented in the ABAQUS platform using a user material subroutine (UMAT) in which the coupling calculation of the stress field and damage field is taken into account. Third, the aforementioned method is applied to predict a real scarf bolted joint of an aircraft fuselage as an engineering application. Furthermore, fatigue experiments of the scarf bolted joints are conducted to validate the performance of the proposed approach. Finally, the effects of three types of factors including the scarf angle, the surface friction between the scarf plates, and the clamping force of bolt are investigated. In addition, the sensitivity of the fatigue life with respect to the scarf angle, surface friction and clamping force is also evaluated.

2. Theoretical models

The CDM based method is used to predict the crack initiation life of the components, which includes two types of theoretical models: the damage-coupled elastic-plastic constitutive model and the fatigue damage evolution model.

2.1. Damage-coupled elastic-plastic constitutive model

In essence, the damage of metal materials is the generation and growth of micro-voids or micro-cracks within the material. The deterioration of the material can be represented by the damage variable in the framework of continuum damage mechanics. Lemaitre and Chaboche [27] presented some fundamental concepts related to continuum damage mechanics. In engineering, the mechanics of a continuous media can be described by a representative volume element (RVE) in which all properties are represented by homogenized variables. For isotropic materials, the damage variable D is used to represent the stiffness deterioration of the RVE and is expressed by

$$D = \frac{E - E_D}{E} \tag{1}$$

where E is the Young's modulus of material and E_D is the effective Young's modulus of the RVE with damage. As E_D ranges from E to 0, D varies between 0 and 1.

For the cases of small deformations, total strain ε_{ij} can be decomposed as

$$\varepsilon_{ij} = \varepsilon_{ij}^e + \varepsilon_{ij}^p \tag{2}$$

where ε_{ij}^e and ε_{ij}^p are elastic strain and plastic strain, respectively. In the damage-coupled constitutive model, damage is coupled with elasticity and plasticity using the effective stress instead of the stress in the elasticity law and the von Mises yield criterion based on the hypothesis of the strain equivalent [23]. The elastic strain takes the form

$$\varepsilon_{ij}^e = \frac{1+\upsilon}{E}\left(\frac{\sigma_{ij}}{1-D}\right) - \frac{\upsilon}{E}\left(\frac{\sigma_{kk}\delta_{ij}}{1-D}\right) \tag{3}$$

where E, v and σ_{ij} are the Young's modulus, the Poisson's ratio and the stress components, respectively. The evolution of the plastic strain is defined as

$$\dot{\varepsilon}^p = \dot{\lambda}\frac{\partial f}{\partial \sigma_{ij}} \tag{4}$$

where $\dot{\lambda}$ is the plastic multiplier. The nonlinear kinematic hardening model proposed by Chaboche [28] is used to represent the kinematic hardening behaviour. The von Mises yield function f with damage is expressed as

$$f = \sqrt{\frac{3}{2}\left(\frac{S_{ij}}{1-D} - \alpha_{ij}\right)\left(\frac{S_{ij}}{1-D} - \alpha_{ij}\right)} - Q \quad \text{where} \quad \alpha_{ij} = \sum_{k=1}^{M}\alpha_{ij}^{(k)} \tag{5}$$

where S_{ij} is the deviatoric part of the stress, and α_{ij} is the deviatoric part of the back stress. Q is the radius of the yield surface, and its evolution is defined as

$$\dot{Q} = \dot{\lambda} b(Q_\infty - Q) \tag{6}$$

where parameters b and Q_∞ are material constants. $\dot{\lambda}$ can be determined by the plastic flow consistency condition: $f = \dot{f} = 0$. The evolution of the plastic strain components [29] can be obtained as

$$\dot{\varepsilon}^p = \frac{3}{2}\frac{\dot{\lambda}}{1-D}\frac{S_{ij}/(1-D) - \alpha_{ij}}{\left(S_{ij}/(1-D) - \alpha_{ij}\right)_{eq}} \tag{7}$$

$$\dot{p} = \sqrt{\frac{2}{3}\dot{\varepsilon}_{ij}^p\dot{\varepsilon}_{ij}^p} = \frac{\dot{\lambda}}{1-D} \tag{8}$$

$$\dot{\alpha}_{ij}^{(k)} = (1-D)\left(\frac{2}{3}C_k\dot{\varepsilon}_{ij}^{p} - \gamma_k\alpha_{ij}^{(k)}\dot{p}\right) \tag{9}$$

where $\dot{p}$ is the accumulated plastic strain rate. C_k and γ_k are material constants that can be determined from experimental tests.

2.2. Fatigue damage evolution model

Plastic deformations may occur in the local area around the notch due to stress concentrations. Therefore, two fatigue damage models are used to calculate the elastic damage and plastic damage. According to the analysis by Kang et al. [30], the total material damage can be decomposed into two parts: the elastic damage and the plastic damage. The elastic damage is dependent on the state of the cyclic stress and the plastic damage is governed by the accumulated plastic strain over each fatigue cycle. The damage evolution rate $\dot{D}$ can be obtained by

$$\dot{D} = \dot{D}_e + \dot{D}_p \tag{10}$$

It should be noted that, in Eq. (10), three forms are typically adopted according to three cases. For the first case, the total damage of the material involves only the elastic damage part given just elastic deformation occurs in the material. For the second case, the total material damage involves only the plastic damage part given the plastic deformation is obvious, and the elastic deformation is relatively so small such that it can be neglected approximately. In the last case, the total damage must be written in the form of Eq. (10) because the elastic damage is almost equivalent to the plastic damage in this scenario. The first two cases will be used for the calibration of damage parameters. The details are presented in the following sections.

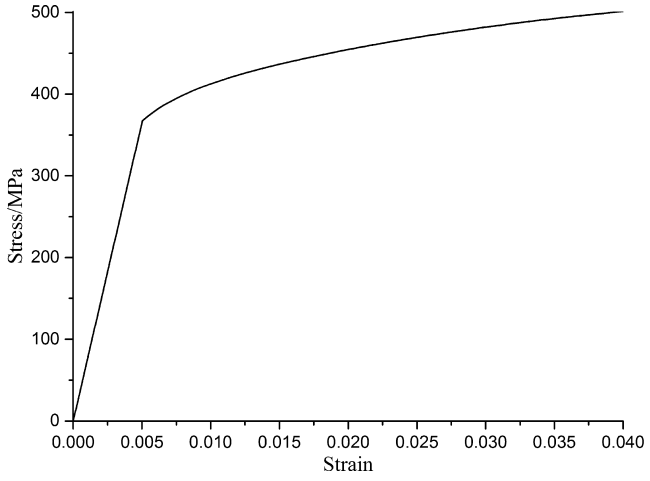

Fig. 1. Stress-strain curve for the 2024-T351 aluminium alloy.

For multiaxial cyclic loading, the elastic damage evolution equation [31,32] of the non-linear continuum damage model can be written as

$$\dot{D}_e = \frac{dD_e}{dN} = \left[1-(1-D)^{\beta+1}\right]^{\alpha}\cdot\left[\frac{A_{II}}{M_0(1-3b_2\sigma_{H,m})(1-D)}\right]^{\beta} \tag{11}$$

where N is the number of cycles until failure, and α, β, M_0 and b_2 are material constants that are determined by fatigue tests, which are explained later on in Section 2.3.2. A_{II} is the amplitude of the octahedral shear stress defined by

$$A_{II} = \frac{1}{2}\left[\frac{3}{2}(S_{ij,\max} - S_{ij,\min})\cdot(S_{ij,\max} - S_{ij,\min})\right]^{1/2} \tag{12}$$

where $S_{ij,\max}$ and $S_{ij,\min}$ are the maximum and the minimum values of the deviatoric stress tensor ij components during one loading cycle. $\sigma_{H,m}$ is the mean hydrostatic stress defined by

$$\sigma_{H,m} = \frac{1}{6}[\max(tr(\sigma)) + \min(tr(\sigma))] \tag{13}$$

where $tr(\sigma) = \sigma_{11} + \sigma_{22} + \sigma_{33}$.

The parameter α is defined by

$$\alpha = 1 - a\left\langle\frac{A_{II} - A_{II}^{*}}{\sigma_u - \sigma_{e,\max}}\right\rangle \tag{14}$$

where $\sigma_{e,\max}$ is the maximum equivalent stress over a loading cycle. The Sines fatigue limit criterion A_{II}^{*} in this model is formulated by

$$A_{II}^{*} = \sigma_{l0}(1 - 3b_1\sigma_{H,m}) \tag{15}$$

The plastic damage evolution equation can be written as

$$\dot{D}_p = \left(\frac{\sigma_{eq}^2 R_v}{2ES(1-D)^2}\right)^{s}\dot{p} \tag{16}$$

where σ_{eq} is the equivalent stress, and $\dot{p}$ is the rate of accumulated plastic strain. S and s are material parameters. R_v is the triaxiality function $R_v = \frac{2}{3}(1+\mu) + 3(1-2\mu)\left(\frac{\sigma_H}{\sigma_{eq}}\right)^2$, and σ_H is the hydrostatic stress.

2.3. Material parameter calibration

The material 2024-T351 aluminium alloy was studied in this paper. According to the experimental data from the uniaxial tensile, low-cycle and high-cycle fatigue tests, two groups of material parameters need to be calibrated: (i) the material parameters in the elastic–plastic constitutive model and (ii) the material parameters in the elastic–plastic damage evolution model. The calibration method is briefly introduced here.

Table 1
Chemical composition of 2024-T351 (wt%).

Si	Fe	Cu	Mn	Mg	Ti	Zn	Al
0.5	0.5	4.9	0.9	1.8	0.15	0.25	Base

Table 2
Static mechanical and material parameters.

E (MPa)	v	σ_y (MPa)	C_1 (MPa)	C_2 (MPa)	γ_1	γ_2
73,000	0.3	385	9250	5360	375	34

Table 3
Material parameters in the elastic-plastic damage model.

Parameters in the elastic damage model					Parameters in the plastic damage model	
β	M_0	b_1	b_2	α	S (MPa)	m
2.15	49,978	0.0007	0.00001	0.75	4.3	3.9

2.3.1. Material parameter calibration in the damage-coupled elastic–plastic constitutive model

According to the uniaxial tensile test, the stress-strain curve can be obtained as shown in Fig. 1, and then, the parameters in the constitutive equations are determined. In this study, the isotropic hardening was neglected, and two components of the back stress were enough to represent the nonlinear kinematic hardening behaviour, which can be expressed as an exponential saturation equation as follows

$$\sigma = \sigma_y + \sum_{k=1}^{2} \frac{C_k}{\gamma_k}(1 - e^{-\gamma_k \varepsilon_p}) \tag{17}$$

where σ_y and ε_p are the initial yield stress and the plastic strain, respectively. The least squares method was used to calibrate parameters. The chemical composition of 2024-T351 is presented in Table 1, and the calibrated parameters are presented in Table 2.

2.3.2. Material parameter calibration in the elastic-plastic damage evolution model

For the case where only of elastic damage occurred, by integrating Eq. (11) from $D = D_0$ to $D = 1$ under the cyclic loading with constant amplitude, where D_0 is the initial damage and is set to be zero in general, the number of cycles to failure N_F can be obtained as

$$N_F = \frac{\{1 - [1 - (1 - D_0)^{\beta+1}]^{1-\alpha}\}}{1+\beta} \cdot \frac{1}{aM_0^{-\beta}} \frac{\langle \sigma_u - \sigma_{e,,\max} \rangle}{\langle A_{II} - A_{II}^{*} \rangle} \cdot \left(\frac{A_{II}}{1 - b_2 \sigma_{H,m}} \right)^{-\beta} \tag{18}$$

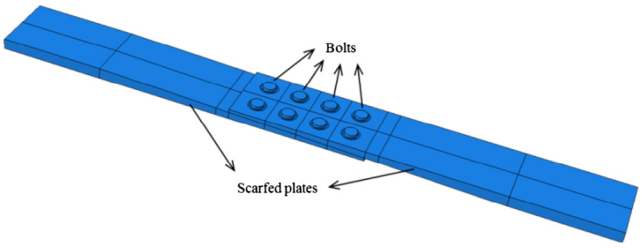

Fig. 2. The scarf bolted joint.

There are five parameters, β, a, M_0, b_1 and b_2 in the elastic damage evolution equation. The four material parameters (β, $1/((1+\beta)aM_0^{-\beta})$, b_1 and b_2) can be determined from the fatigue experimental data of smooth specimens. For the case of smooth specimens under uniaxial fatigue loading, a closed form expression of fatigue life can be derived: $N_F = \frac{1}{1+\beta} \cdot \frac{1}{aM_0^{-\beta}} \frac{\langle \sigma_u - \sigma_{\max} \rangle}{\langle \sigma_{\max} - \sigma_{l0} \rangle} \cdot (\sigma_a)^{-\beta}$. Therefore, parameters β and $1/((1+\beta)aM_0^{-\beta})$ are readily identified from the fatigue test data with $R = -1$. Then, using the least squares method, parameters b_1 and b_2 can be obtained from the fatigue tests data at other stress ratios.

Finally, the independent parameters a and M_0 were identified numerically on the basis of the damage mechanics–finite element method [33–35]. The fatigue experimental data of material 2024-T351 were found in the literature [36]. The calibrated parameters for the elastic damage evolution model are listed on the left side of Table 3.

There are two parameters, m and S, in the plastic damage evolution model that can be calibrated from the strain-controlled low-cycle fatigue test data. According to the Coffin-Manson law, the strain-life curve can be expressed as

$$\frac{\Delta \varepsilon_p}{2} = \varepsilon_f' (2N_f)^c \tag{19}$$

where ε_f' and c are the material parameters. For the uniaxial case, the number of cycles until failure can be obtained by integrating Eq. (16) from $D = 0$ to $D = 1$

$$N_f = \frac{1}{2(2m+1)\Delta \varepsilon_p} \left(\frac{2ES}{(\sigma_{\max})^2} \right)^m \tag{20}$$

Using the cyclic stress–strain curve described as

$$\sigma_{\max} = K' \left(\frac{\Delta \varepsilon_p}{2} \right)^{n'} \tag{21}$$

where K' and n' are parameters obtained from experiments, Eq. (20) can be expressed as

$$N_f = \frac{1}{2(2m+1)} \left(\frac{2^{1+2n'} ES}{(K')^2} \right) (\Delta \varepsilon_p)^{-(1+2mn')} \tag{22}$$

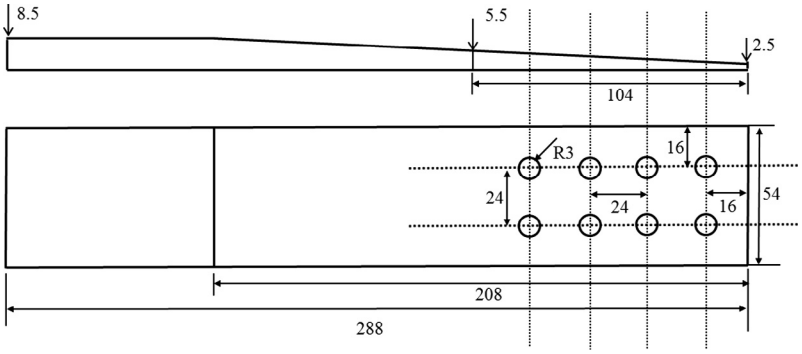

Fig. 3. Geometry of the scarf plate.

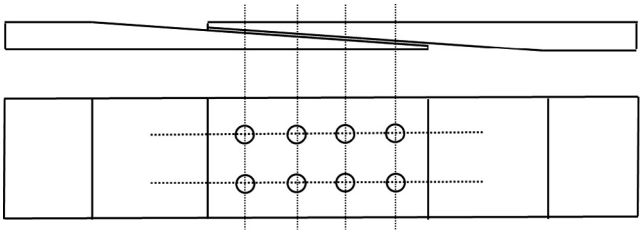

Fig. 4. Schematic diagram of the assembly of the scarf bolted joints.

Table 4
Fatigue experimental results for the scarf bolted joints.

Specimen No.	Fatigue life/cycle	Specimen No.	Fatigue life/cycle
1	85,605	7	267,472
2	160,003	8	567,472
3	290,671	9	146,765
4	146,657	10	365,371
5	144,512	11	267,925
6	145,635		
Experimental mean life		235,280	

The values of ε_f', c, K' and n' are obtained from the low-cycle fatigue tests data [37]. The parameters in the plastic damage evolution model are listed in Table 3.

3. Fatigue life prediction for the scarf bolted joint

3.1. Fatigue experiments for the scarf bolted joint

The scarf bolted joint consisted of one pair of scarf plates and four pairs of bolts, as shown in Fig. 2. The scarf plate was made of 2024-T351 aluminium alloy, and the geometry is illustrated in Fig. 3. The length was 288 mm, and the width was 54 mm. The thickness of the clamping piece was 8.5 mm, and the minimum thickness of the scarf plate was 2.5 mm; thus, the scarf angle α_{scarf} was approximately 1.65°. In the experiments, the contact surfaces of the plates were polished using sandpapers with different grits (400, 600, 800, and 1000), to obtain a smooth surface. The scarf plates were connected by the countersunk bolts, which were made of TC18 titanium alloy. The diameter of bolt hole was 6 mm and the diameter of the bolt was 5.88 mm. Thus, a clearance fit existed between the bolt and hole. Meanwhile, the specimen was always subjected to the tensile-tensile fatigue cyclic loading, so the hole and the bolt keep contacting on the one side of the hole surface during the experiments. The distance between two bolt holes was 24 mm. The clamping force is 5 kN. In the experiments, the bolts were applied tightening torque by using a Norbar torque wrench. Generally, the assumption is acceptable that a certain tightening torque can develop an identical clamping force for the same type of joints. In some Refs. [7,11,38], studies have shown that an almost perfectly linear relation exists between the tightening torque and the resulting clamping force. In the experiments, we didn't measure the clamping force, which was calculated according to an empirical equation [39,40]: $F_{cl} = \frac{T_{cl}}{k_{cl} d_{bolt}}$, where F_{cl} is the initial clamping force, T_{cl} is the torque, k_{cl} is the torque factor and d_{bolt} is the bolt diameter. A schematic diagram of the assembly of the scarf bolted joints is shown in Fig. 4.

Specimen fatigue experiments were carried out using the MTS fatigue testing machine, and the frequency was 3.5 Hz. The maximum load was 35 kN. The maximum stress during a loading cycle was 90 MPa and the stress ratio was 0.06. In the design of aircraft structures, the statistical data scatter of the fatigue life due to the sample size and reliability level must be considered. The 95% confidence level for a fatigue life at a specified stress level was used, which ensures that there was a 95% possibility of survival or reliability. The experimental results are presented in Table 4. The fracture photograph of the scarf plate is shown in Fig. 5. In the experiment, the crack nucleation point was not determined because it is difficult to observe the accurate crack initiation locations which are usually at the edge of bolt hole on the contact surface of the scarf plates. However, it can be deduced from the crack path that the crack nucleated from the edge of the hole and the site was approximately of the angle of 90° relative to the tension loading. In addition, according to the fatigue experimental results for the scarf bolted joint, there were not obvious fretting marks on the contacting surfaces which indicates that the relative movement between the plates was not notable, thus we didn't conduct the calculation of fretting damage in the study.

3.2. Numerical algorithm

The user subroutine UMAT in ABAQUS was used to implement the damage-coupled elastic–plastic constitutive model and the damage evolution equations and to conduct the initiation life prediction. The flowchart of the numerical calculation is illustrated in Fig. 6, and the detailed steps are the following:

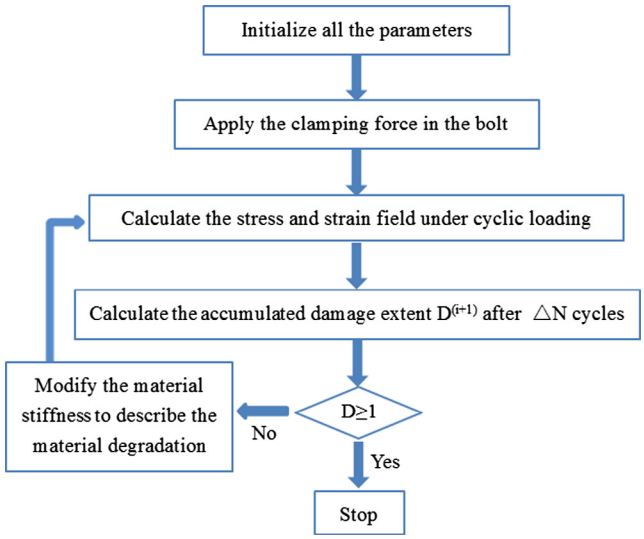

Fig. 6. The flowchart of the numerical calculation.

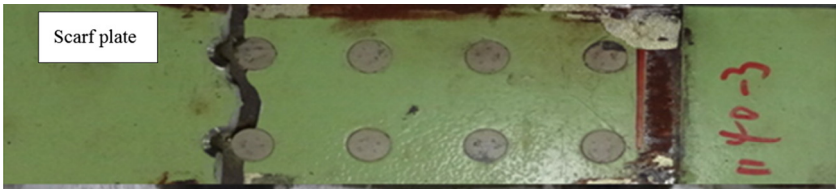

Fig. 5. Fracture photograph of the scarf plate.

(1) Initialize all the parameters to be 0 and apply the clamping force in the bolt.

(2) The cyclic stress and the accumulated plastic strain were calculated using ABAQUS software under cyclic loading and residual stress field. For the case of the elastic damage accumulation, as it is time consuming to calculate the fatigue damage cycle by cycle, the jump-in-cycles procedure [41,42] was adopted in the numerical implementation, which assumes that the cyclic stresses and the accumulated plastic strain and damage increment remain unchanged for each cycle during each block of ΔN cycles. Each block consists of 200 cycles in this study. It is necessary to note that the value of ΔN is determined to obtain a convergent fatigue life. Generally, according to the literature [33,43], the value of ΔN is applicable when it satisfies the condition of $\Delta N/N_f \leq 0.01$. However, for the case of elastic-plastic damage accumulation, the damage increment should be calculated cycle by cycle because the accumulated plastic strain may be distinct for each cycle. Then, the increment of the fatigue damage is calculated as

$$\Delta D^{(i+1)} = \begin{cases} \Delta N \cdot \dot{D}_e^{(i+1)}, only\ elastic\ damage\ occurs \\ \dot{D}_e^{(i+1)} + \dot{D}_p^{(i+1)}, elastic-plastic\ damage\ occurs \end{cases} \quad (23)$$

Then, the total extent of damage corresponding to the total loading cycle of N is obtained as

$$D^{(i+1)} = D^{(i)} + \Delta D^{(i+1)} \quad (24)$$

(3) If the accumulation of damage at any element reaches 1, a fatigue crack initiates at this element, and the corresponding number of cycles is the fatigue crack initiation life, or else, a recalculation of the material properties of each element is conducted using the following equation

$$E^{(i+1)} = E^{(i)}(1 - D^{(i+1)}) \quad (25)$$

Then, the analysis of the stress field and the damage field is repeated until the accumulation of damage at any element reaches 1. The crack initiation life is predicted. For the case of the damage value greater than zero but less than 1, it indicates that the material was damaged but not failure, and the damage state of material is reflected by reducing the effective elastic modulus of RVE.

3.3. Finite element model

In the ABAQUS platform, only half of the scarf bolted joint was built using a symmetric boundary condition at the plane of symmetry. The model of the component consisted of one pair of scarf

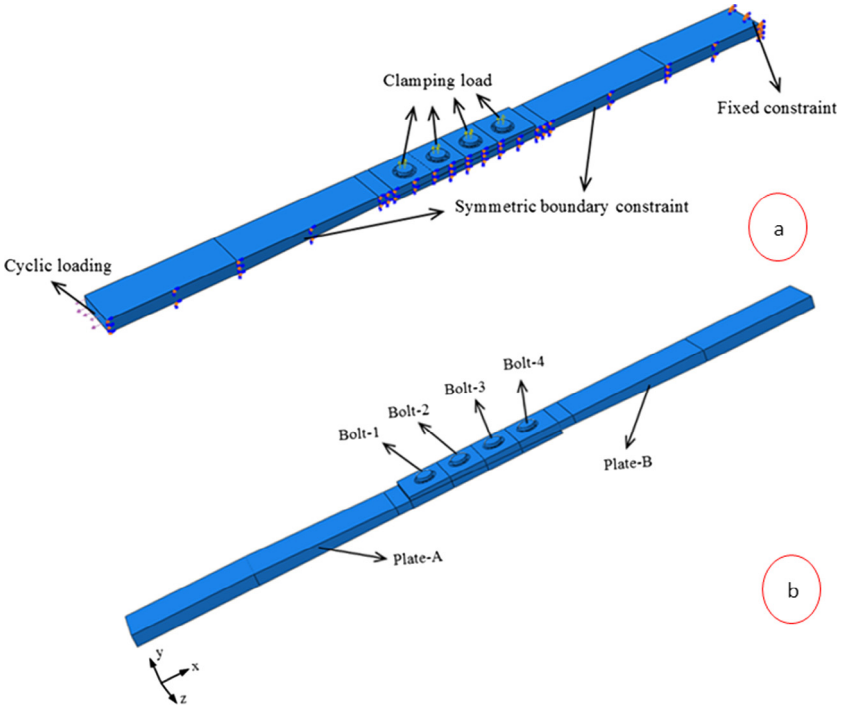

Fig. 7. One half of the model: (a) loads and constraint conditions and (b) schematic diagram of coordinate system and part name.

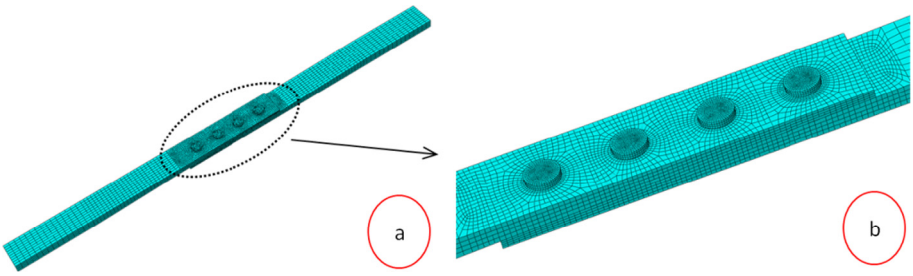

Fig. 8. The established finite element model: (a) the global view and (b) the local view.

plates and four bolts, as shown in Fig. 7(a). Cyclic loading was applied along the axial direction of the scarf plates, which is simply the x direction of the coordinate system, as shown in Fig. 7(b). A 3D 8-node linear solid element (C3D8) in ABAQUS was used to mesh the scarf plates and bolts. The element is defined by eight nodes with three degrees of freedom for each node: translations in the nodal directions, x, y, and z. To accurately obtain the stress field in the local contact zone between the scarf plate and the bolt, a high quality mesh discretization was performed. A mesh sensitivity analysis was also conducted to obtain a convergent solution independent of the FE mesh size in the numerical computation. The meshes around the bolt hole were refined with a minimum mesh size of 0.1 mm^3. A total of 199,032 elements were created. The meshed FE model is shown in Fig. 8.

The damage-coupled elastic-plastic constitutive model was adopted to simulate the stress-strain behaviour of the scarf plate, and a linear elastic material behaviour is used to simulate the stress-strain behaviour of bolt with an elastic modulus of 110 GPa and a Poisson's ratio of 0.3. The contacts between the surfaces of scarf plate and bolt and two surfaces of scarf plates were defined using the master-slave algorithm. The contact pair is composed of a master surface and a slave surface. The normal direction of a pair of the contact surfaces is reversed, that is, the normal direction of a master (or slave) surface points to the slave (or master) surface. The tangential direction of a surface is perpendicular to the normal direction, and the tangential direction of a pair of the contact surfaces is also reversed. The sliding formulation was set as finite sliding. In the FE simulation, it is important and representative to use the stabilized coefficient of friction [44,45]. In this study, the coefficient of friction was not measured in the experiment. The stabilized coefficient of friction $\mu = 0.65$ from Refs. [46,47] was used for the pair of scarf plates, and the coefficient of friction between the scarf plates and bolt was set to be 0.2 [13]. In the numerical simulation, the clamping load was first applied to the bolt section, and then the cyclic loading was applied at the end of the scarf plate. The clamping force F_{cl} was 5 kN, and the maximum stress in a loading cycle was 76.25 MPa with a stress ratio of 0.06.

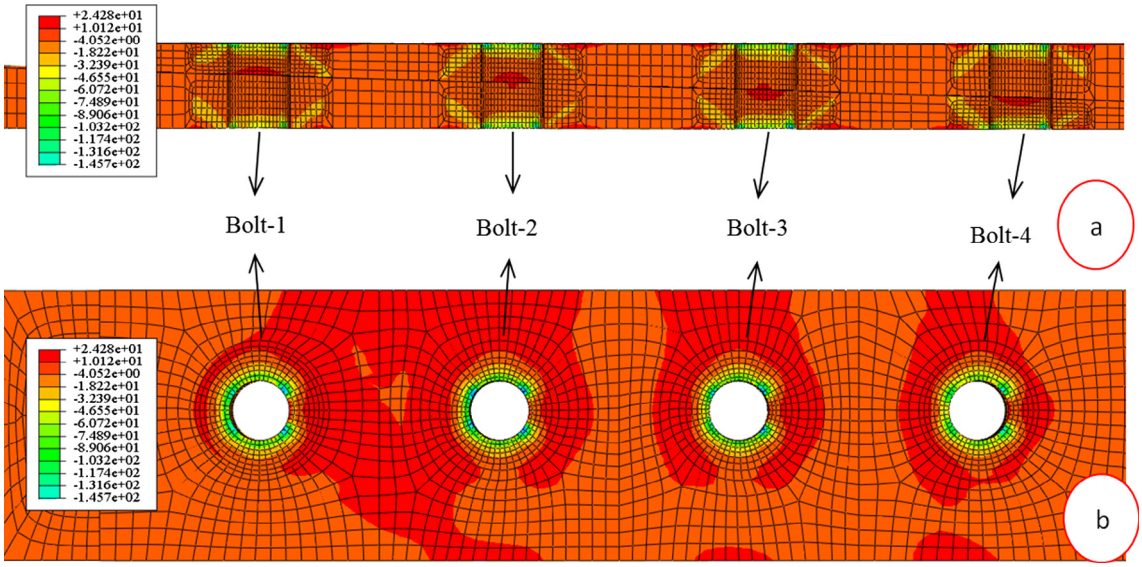

Fig. 9. Distribution of the longitudinal stress (MPa): (a) along the depth direction on the area around the bolt hole and (b) on the surface of the plate.

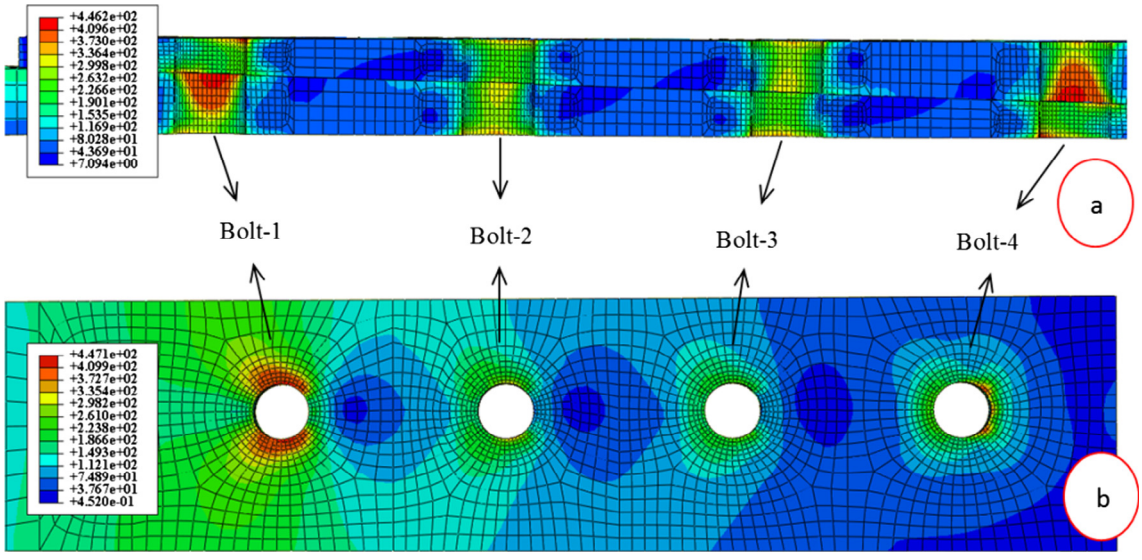

Fig. 10. Distribution of the von Mises stress (MPa): (a) along the depth direction on the area around the bolt hole and (b) on the contact surface of the scarf plates.

It is worth noting that for the case of our study, the clamping force and the friction coefficient adopted in the manuscript can be considered as an acceptable approximation compared to the experimental values. Thus, we tried to present the readers a verified model before the sensitivity analysis of factors.

3.4. Computational results

After the application of the clamping force, the distribution of the longitudinal stress (i.e. the stress along the longest feature of the plate) on the bolt hole was obtained, as shown in Fig. 9, which indicates that the compressive stress occurs at the edge of the bolt hole, which is favourable for the fatigue life of the scarf plate by decreasing the mean stress value of the local area when the joint is subjected to the cyclic loading. In Section 4.3, the effects of different clamping forces on the fatigue life are discussed. The distribution of the von Mises stress on the scarf plates under the clamping force and the cyclic loading is presented in Fig. 10, which shows that (1) the von Mises stress decreases along with an increase in the distance away from the hole edge for every bolt hole, (2) the stress values on bolt-1 hole and bolt-4 hole are greater than on other bolt holes, (3) the maximum value of stress on the bolt hole occurs at the contact surface of the two scarf plates, which may be the position where the fatigue crack initiates.

Based on the proposed numerical algorithm, the calculated fatigue life of the scarf bolted joint was 267,510. Fig. 11(a) shows the calculated fatigue damage field of the local area and the crack initiation site for the scarf bolted joint. The results show that the crack initiates at the contact surface of the two scarf plates on the hole of bolt-1. The extent of the damage versus the number of cycles for the critical element is shown in Fig. 11(b), and Fig. 11(c) shows the evolution of the elastic damage rate dD_e/dN. According to the calculated results, the total plastic damage D_p was approximately 0.1, and the total elastic damage D_e was approximately 0.9; thus, the elastic damage was dominant in the fatigue damage process of the material, which is reasonable considering that the calculated fatigue life lies in the high cycle fatigue region. Fig. 12 shows the calculated evolution curve of the von Mises stress versus the number of cycles at the critical element under the fatigue loadings. We can see that the maximum stress decreases as the number of loading cycles increases, which is caused by the stress redistribution due to the accumulated fatigue damage.

The calculated life is needed to be compared with the experimental life to validate the model. Therefore, it is much necessary to demonstrate the comparability between these two results. On one hand, in the experiments, it is difficult to determine the moment when the cracks initiate due to that the initiation sites

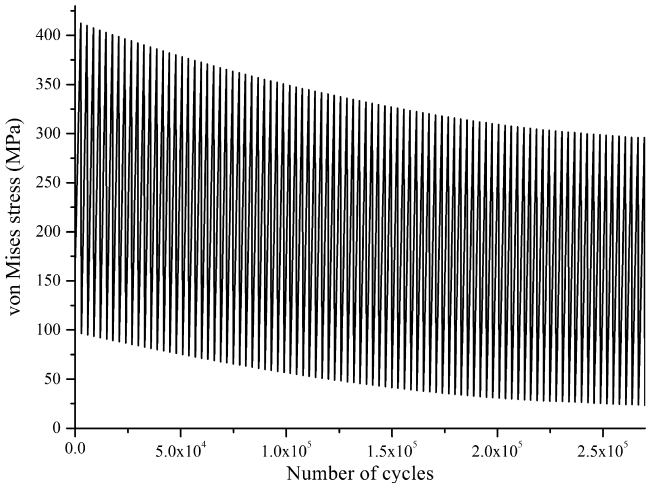

Fig. 12. The evolution curve of the von Mises stress at the critical element versus the number of cycles.

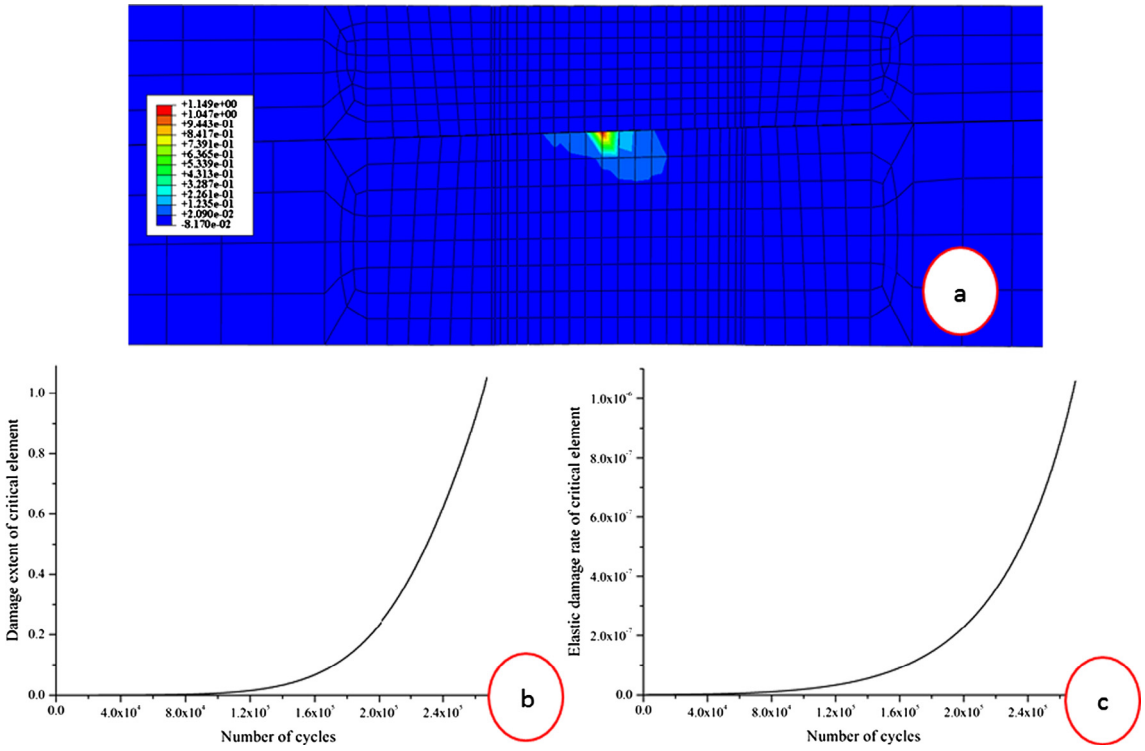

Fig. 11. Fatigue damage analysis: (a) damage field distribution of the local area, (b) the damage extent versus the number of cycles for the critical element and (c) the evolution curve of the elastic damage rate.

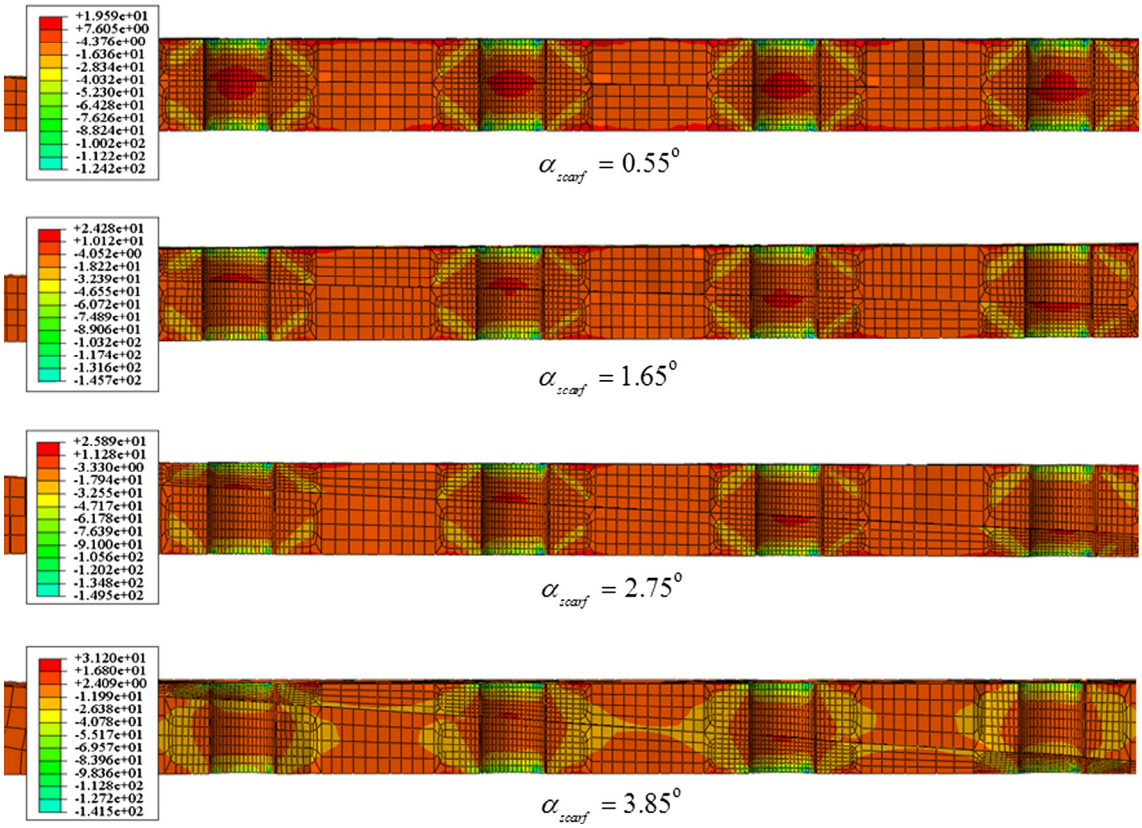

Fig. 13. Distribution of the longitudinal stress (MPa) with respect to different scarf angles.

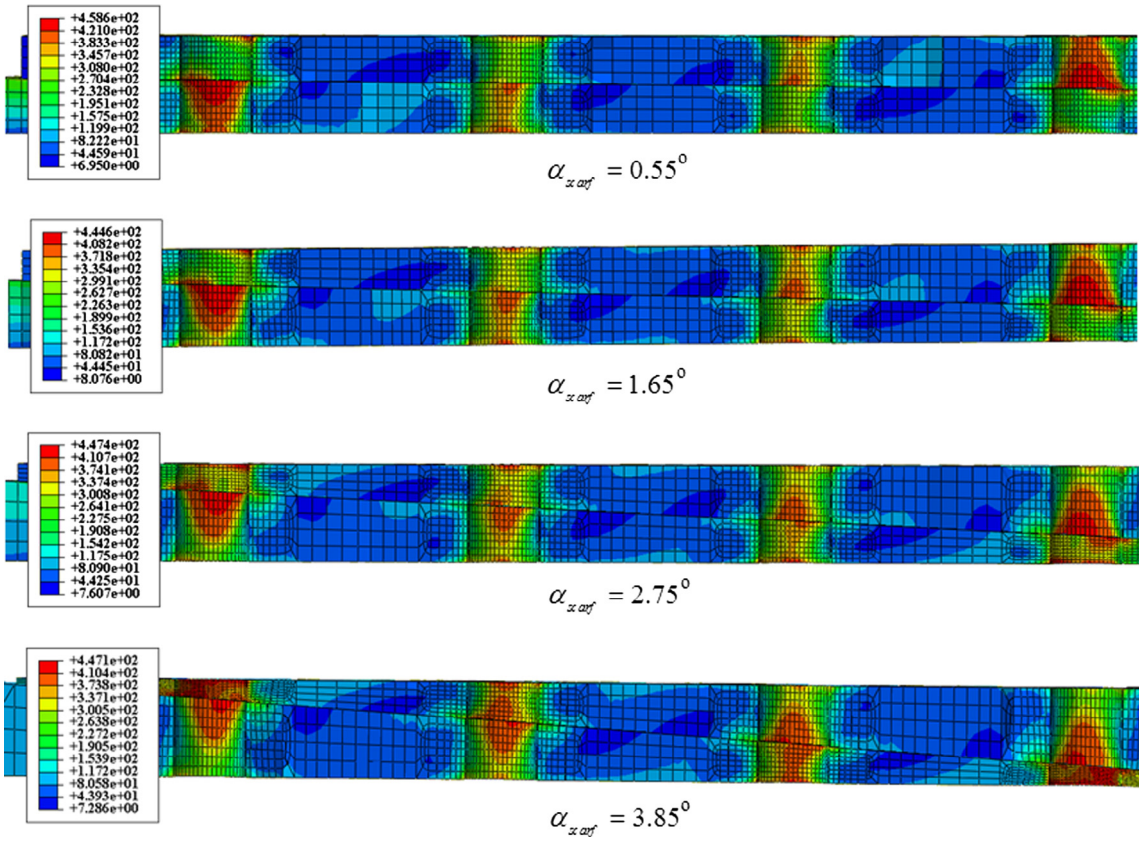

Fig. 14. Distribution of the von Mises stress (MPa) with respect to different scarf angles.

are at the edge of bolt hole on the contact surface of the scarf plates. However, we found that the life corresponding with the end phase of the fracture was relative short by comparing the number of cycles when the crack was small (0.1–1 mm) but could be observed by eyes. Thus, although we cannot test the crack initiation life accurately for each specimen, it is reasonable to assume the experimental life to be approximate the crack initiation life. On the other hand, in the numerical implementation based on the continuum damage mechanics, the crack initiation criterion is that the accumulation of the damage value at any one element reaches 1. The corresponding physical meaning is that the critical element loses the load carrying capacity. Therefore, to some extent, the dimension of the critical element is equivalent to the length of crack initiation. The average size of meshes in the critical zone of the FE model is about 0.08 mm. Thus, the calculated fatigue life can be approximately compared with the experimental result.

The experimental mean life listed in Table 4 is 235,280, and the error between the calculated result and the experimental mean life is 13.7%. It is shown that the calculated result is in accordance with the experimental result, and the calculated result is acceptable for engineering applications.

4. Discussions

This section discusses the effects of the scarf angle, the friction coefficient and the clamping force on the fatigue life of the scarf bolted joint. In addition, a sensitivity analysis of the fatigue life with respect to these three factors is also conducted.

4.1. Effects of the scarf angle

The scarf angles discussed in this section are 0.55°, 1.65°, 2.75° and 3.85°, respectively. The friction coefficient between the scarf plates is set to be 0.65. The clamping force on the bolt is 5000 N, and the maximum stress in a loading cycle is 90 MPa with a stress ratio of 0.06 for all the cases.

4.1.1. Effects on the stress distribution of the bolt hole and on the load transferred by the bolts

After the application of clamping force, the distribution of the longitudinal stress on the bolt hole is shown in Fig. 13. Two important points can be obtained: (1) the distribution rules of the stress are similar for the four scarf angles and (2) the region of compressive longitudinal stress and the maximum value of the compressive longitudinal stress increase along with an increase in the scarf angle, which is favourable for the fatigue life of the scarf plate.

The distribution of von Mises stress on the bolt hole under the clamping force and cyclic loading are shown in Fig. 14. We can see that (1) the distribution rules of the stress are similar for four scarf angles and (2) the maximum value of the von Mises stress occurs on the hole of bolt-1 at the contact surface of the two scarf plates for all the cases, which indicates that the crack may initiate at this

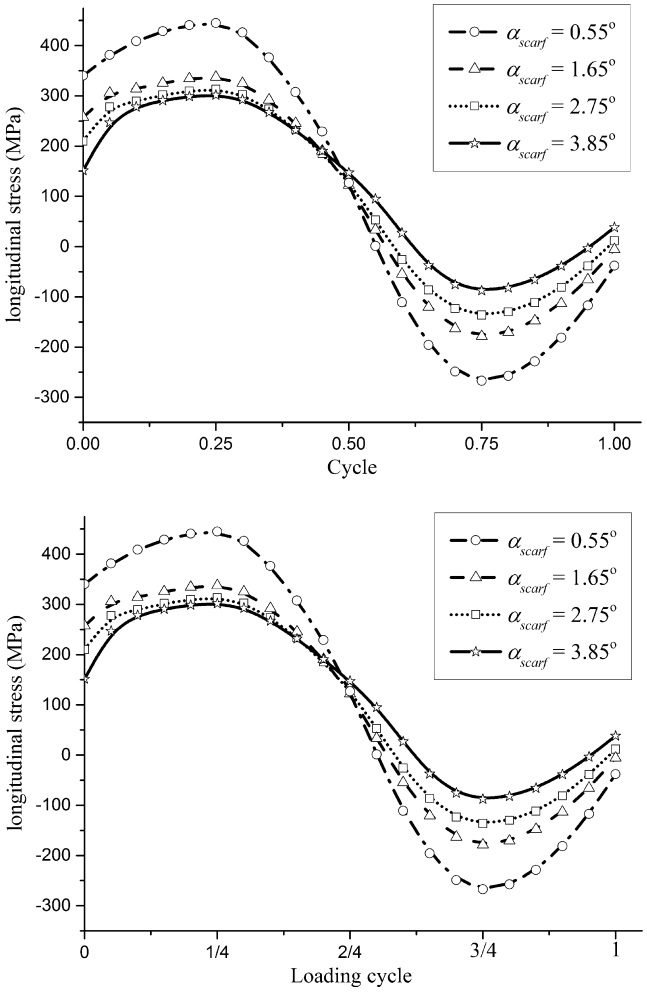

Fig. 15. Change in the longitudinal stresses (MPa) within one loading cycle with respect to different scarf angles.

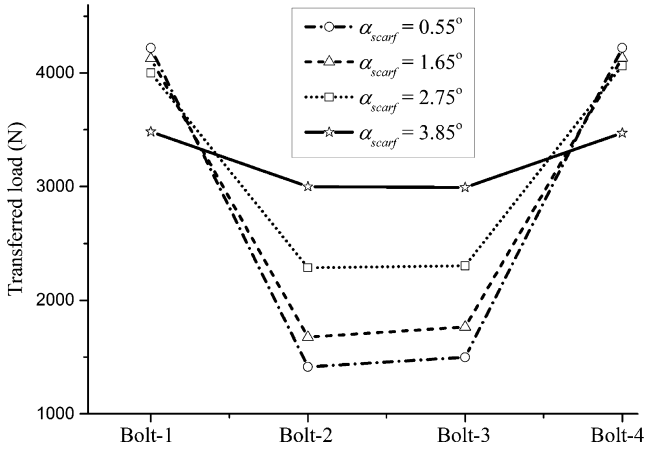

Fig. 16. Effect of the scarf angle on the load transferred by each bolt.

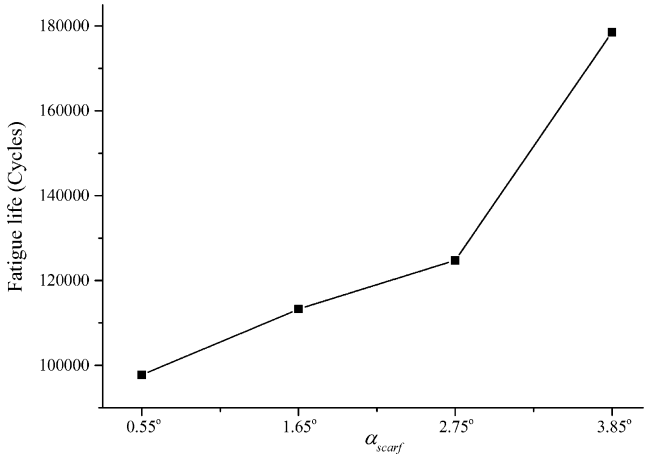

Fig. 17. Fatigue life versus the scarf angle.

position. Fig. 15 shows the change in the longitudinal stress at the critical element within one loading cycle. The stress amplitudes and the maximum stresses are shown to decrease significantly when the scarf angle increases from 0.55° to 3.85°, which is favourable for the fatigue life improvement of the scarf plate.

The loads transferred by the bolts with different scarf angles are presented in Fig. 16, which shows that (1) loads transferred by bolt-1 and bolt-4 (refer to Fig. 7) are dominant and sustain approximately 65% of the total load, (2) loads transferred by bolt-1 and bolt-4 decrease as the scarf angle increases, and (3) loads transferred by bolt-2 and bolt-3 are much smaller and increase along with the increase in the scarf angle. Therefore, a greater scarf angle is favourable for the average of the load transferred by the bolts, which can benefit the fatigue life of the bolt hole.

4.1.2. Effects on the fatigue life

The fatigue lives of the scarf bolted joint with different scarf angles were calculated using the numerical scheme described in Fig. 6. The curve of the fatigue life versus scarf angle is shown in Fig. 17. We can see that a larger the scarf angle results in a longer the fatigue life. For all the cases, the predicted crack initiates at the contact surface of the two scarf plates on the bolt hole. The relationship between the damage extent versus the number of cycles corresponding to the critical element is plotted in Fig. 18(a). As the number of cycle increases, the equivalent Young's modulus of the critical element will decrease, as shown in Fig. 18(b), resulting in the redistribution of the stress. When N reaches N_f, the damage extent at the critical element is close to 1. For each case, the total plastic damage of the critical element is less than 0.15, and the fatigue damage processes of the material are primarily controlled by the elastic damage. The evolution of elastic damage rate dD_e/dN is shown in Fig. 18(c). The failure locations of the critical element corresponding to the different scarf angles are presented in Fig. 19, which shows that the failure locations of the critical elements almost stay the same, which are at the location of 90° on the bolt hole.

On the whole, the main reasons for the changing trend of fatigue life corresponding to different scarf angles are described by the following two aspects: (1) the stress amplitude and maximum stress decrease along with an increase in the scarf angle; and (2) the larger scarf angle can average the load transferred by the bolts and reduce the maximum value of load transferred by bolt-1 and bolt-4 on the ends.

4.2. Effects of the friction coefficient

The friction coefficients between the scarf plates discussed in this section were 0.25, 0.45, 0.65, and 0.85, respectively. The scarf angle was 1.65°. The clamping force on the bolt was 5000 N, and the maximum stress during a loading cycle was 90 MPa with a stress ratio of 0.06 for all cases.

4.2.1. Effects on the stress distribution on the bolt hole and on the load transferred by the bolts

After the application of the clamping force, the distributions and values of the longitudinal stress on the bolt hole were almost the same for each case, as shown in Fig. 20. The distribution of longitudinal stress was closely related to the clamping force and the

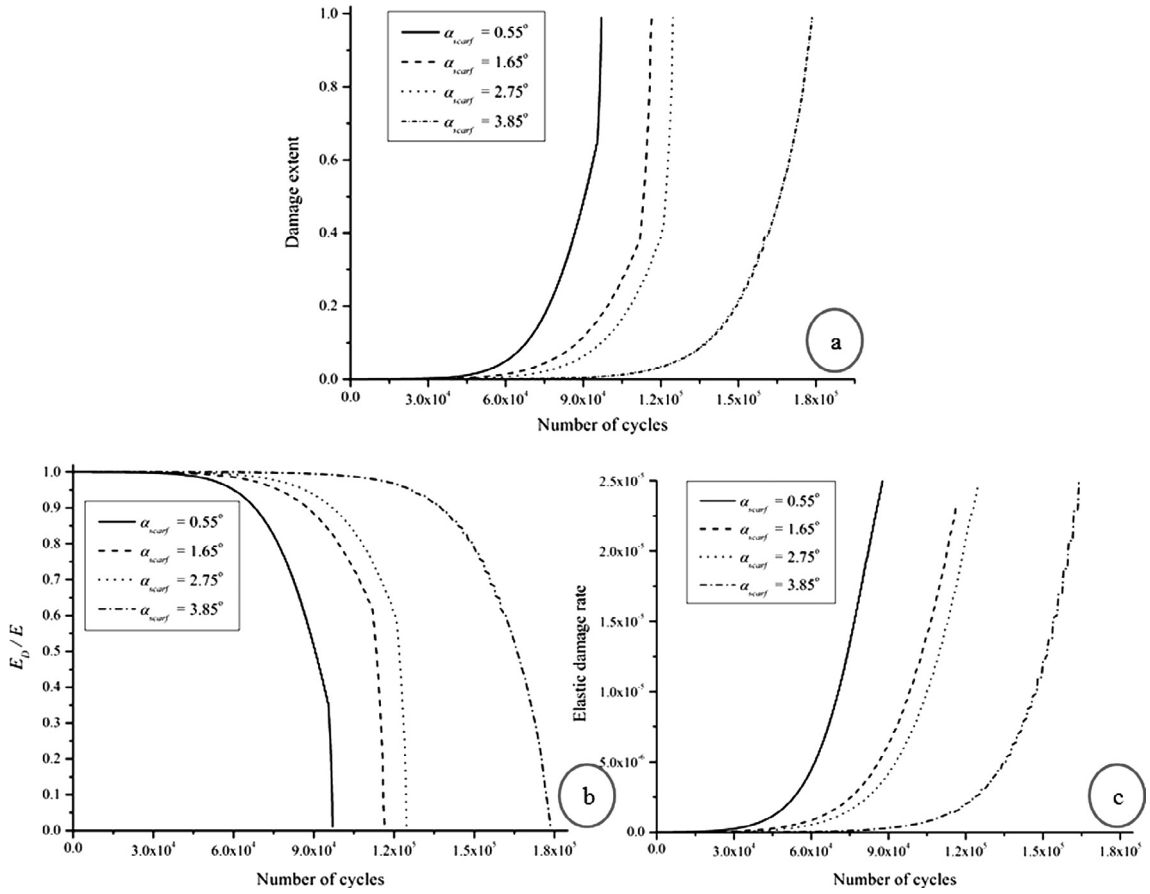

Fig. 18. (a) Damage extent versus the number of cycles with respect to different scarf angles, (b) reduction in the equivalent Young's modulus of the critical element and (c) the evolution curve of the elastic damage rate.

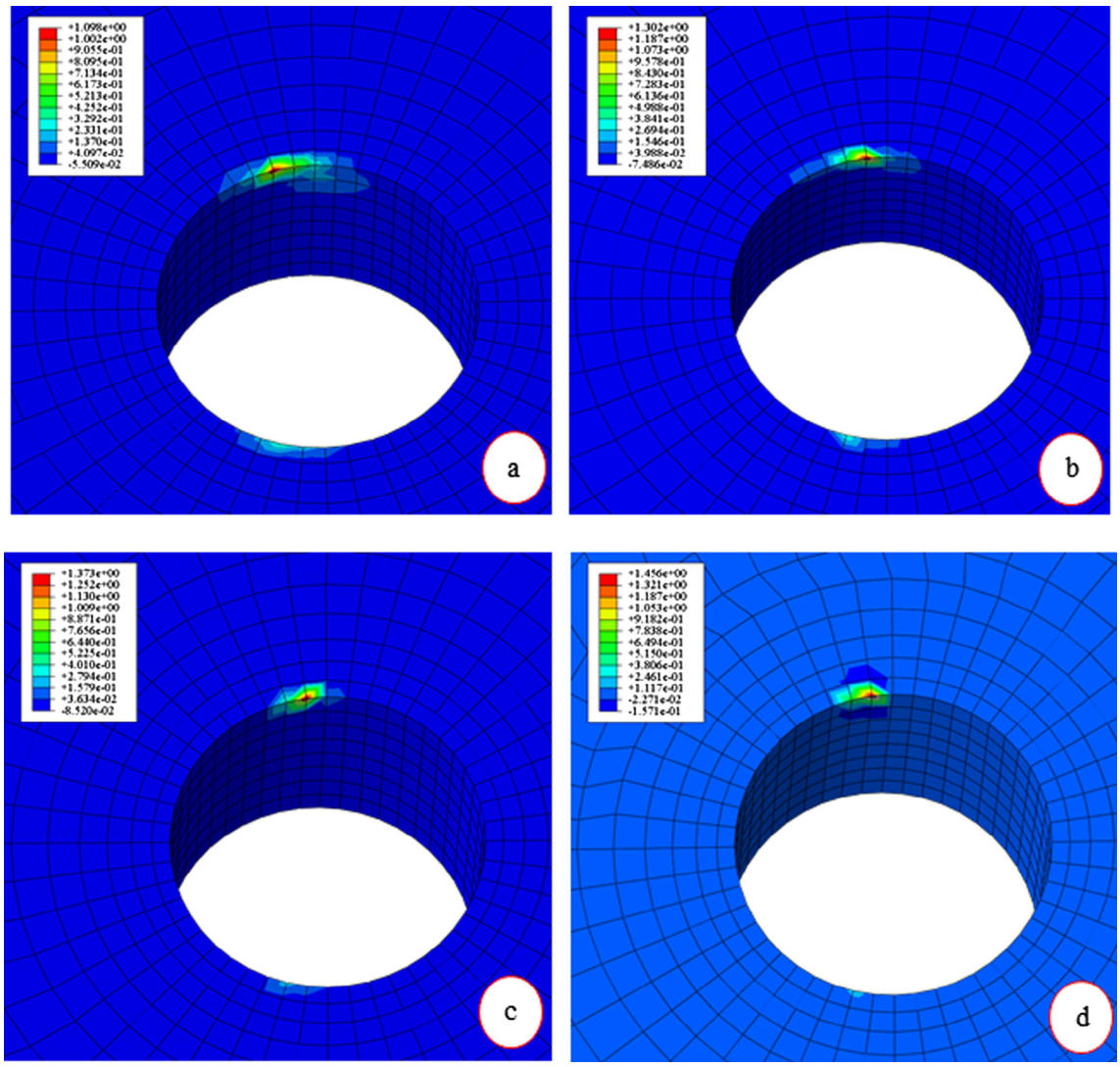

Fig. 19. Failure locations of the critical element corresponding to the different scarf angles (a) scarf angle = 0.55°, (b) scarf angle = 1.65°, (c) scarf angle = 2.75° and (d) scarf angle = 3.85°.

scarf angle; however, the friction between the scarf plates had no effect on the longitudinal stress.

The distributions of the von Mises stress on the bolt hole under the clamping force and cyclic loading are shown in Fig. 21, which indicates that (1) the distribution rules of the stress are similar, and the maximum value of von Mises stress occurs on bolt-1 hole at the contact surface of the two scarf plates for each case, and (2) the region of von Mises stress with greater values on each bolt hole decrease along with an increase in the friction coefficient, which can be favourable for the fatigue life of the scarf plate. Fig. 22 shows the change in the longitudinal stress at the critical location within one loading cycle. Obviously, when the friction coefficient increases from 0.25 to 0.85, the maximum value of the stress changes slightly, while the stress amplitude is shown to significantly decrease, which is favourable for the fatigue life improvement of the scarf plate.

The loads transferred by the bolts with different friction coefficients are presented in Fig. 23(a), which shows that (1) loads transferred by bolt-1 and bolt-4 are dominant and bear the most load, and (2) loads transferred by each bolt decrease markedly when the friction coefficient increases from 0.25 to 0.85. Fig. 23(b) shows the total loads transferred by the bolts and by the frictional force for the bolted joints at different friction coefficients. It is obvious that the friction coefficient increases, the total loads transmitted by the frictional force increases and the total loads transmitted by the bolts decrease. The decrease in the loads transmitted by the bolts leads to a reduction in the stress amplitude at the bolt hole, which is favourable for fatigue life improvement of the scarf plate.

4.2.2. Effects on the fatigue life

The fatigue lives of the scarf bolted joint with different friction coefficients were calculated, and Fig. 24 shows the calculated fatigue life versus the friction coefficient. It is clear that a larger friction coefficient between the scarf plates results in a longer fatigue life. For all cases, the predicted crack initiates at the contact surface of the two scarf plates on the bolt hole. Fig. 25(a) shows the damage extent versus the number of cycles corresponding to the critical element, and Fig. 25(b) shows the reduction of the equivalent Young's modulus at the critical element. The fatigue damage processes of the material for each case are primarily controlled by the elastic damage. The failure locations of the critical elements corresponding to the different friction coefficients are presented shown in Fig. 26, which shows that the failure locations of the crit-

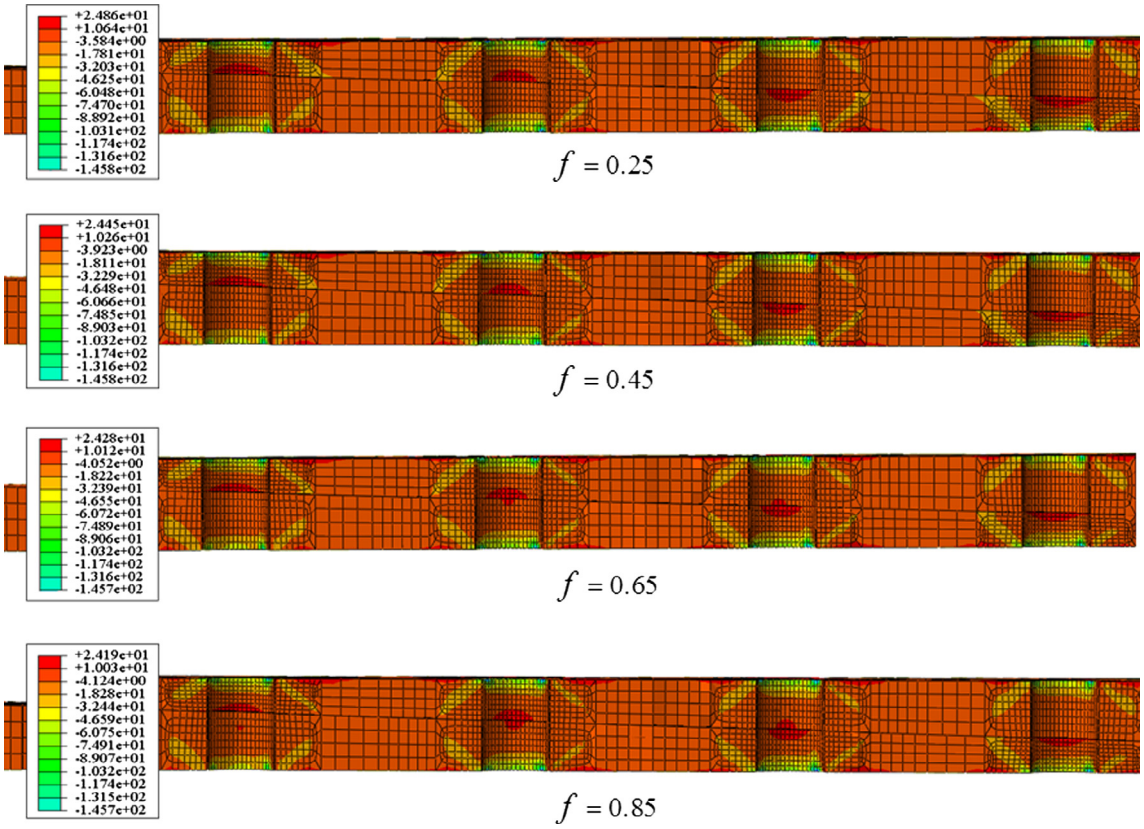

Fig. 20. Distribution of the longitudinal stress (MPa) with respect to different friction coefficients.

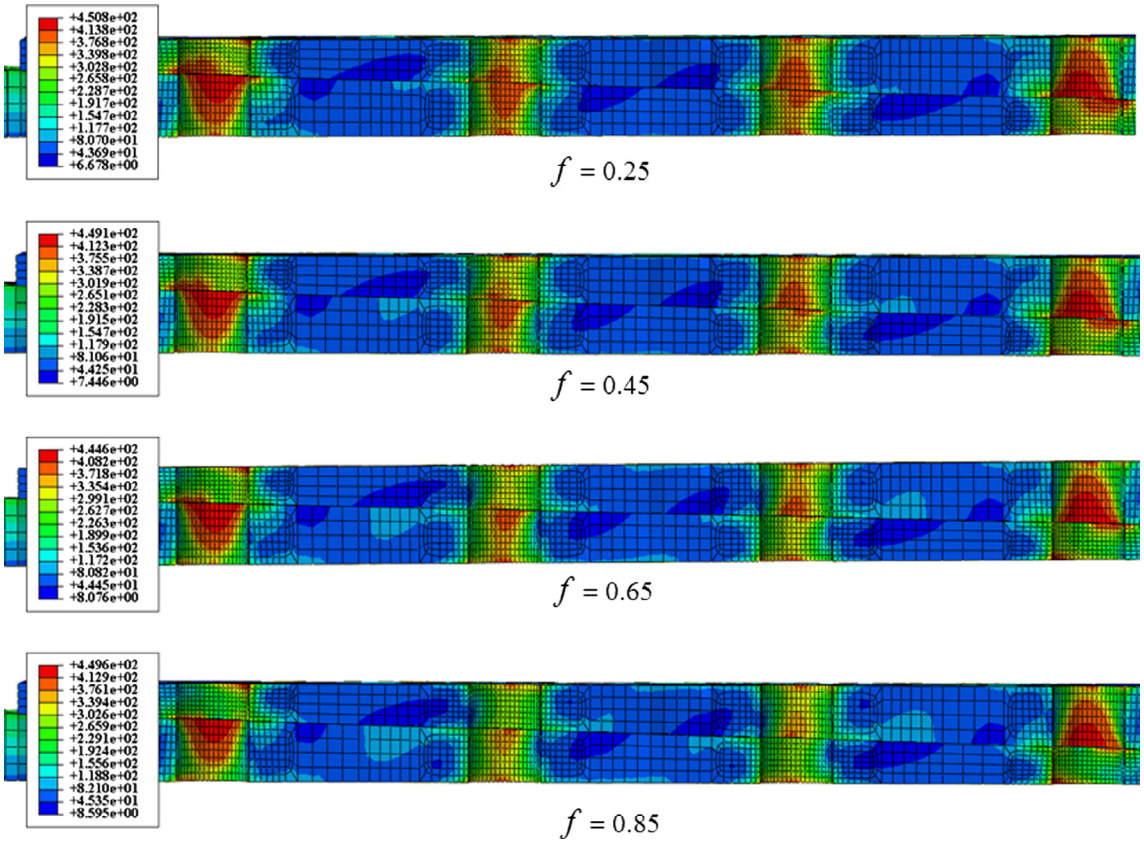

Fig. 21. Distribution of the von Mises stress (MPa) with respect to different friction coefficients.

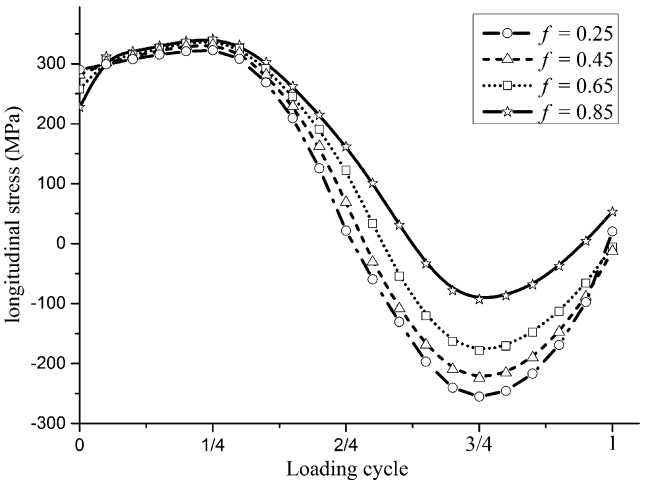

Fig. 22. Change of the longitudinal stresses (MPa) within one loading cycle with respect to different friction coefficients.

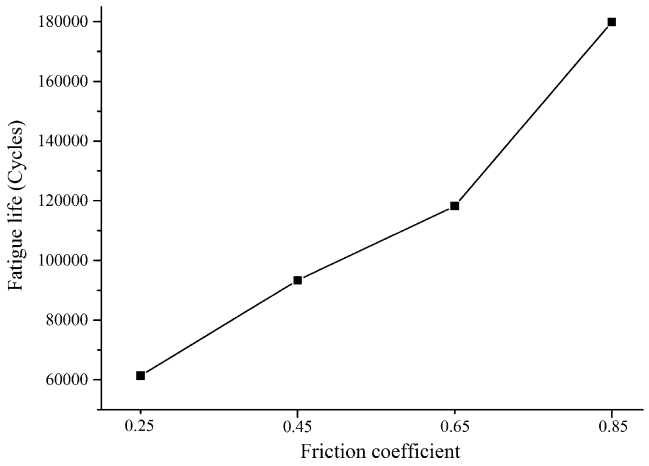

Fig. 24. Fatigue life versus the friction coefficient.

ical elements change a little, however, which are all around the location of 90° on the bolt hole.

On the whole, the main reason for the changing trend of the fatigue life corresponding to different friction coefficient is that, as the friction coefficient increases, the total loads transferred by the frictional force increase and the loads transmitted by the bolts decrease, which lead to the obvious reduction in the stress amplitude of the critical element; thus, the fatigue life increases.

4.3. Effects of the clamping force

The clamping forces applying to the bolts discussed in this section were 0 N, 2000 N, 5000 N and 8000 N, respectively. The scarf angle was 1.65°. The friction coefficient between scarf plates was 0.65, and the maximum stress in a loading cycle was 90 MPa with a stress ratio of 0.06 for all cases.

4.3.1. Effects on the stress distribution on the bolt hole and on the load transferred by the bolts

After the application of the clamping force, the distribution of the longitudinal stress on the bolt hole is shown in Fig. 27, which indicates that the maximum value of the compressive longitudinal stress increased along with an increase in the clamping force. Fig. 28 shows the distribution of the von Mises stress on the bolt hole under the clamping force and cyclic loading. For all the cases, the maximum values of the von Mises stress were similar and occur on the bolt-1 hole at the contact surface of the two scarf plates. Fig. 29 shows the change in the longitudinal stress at the critical element within one loading cycle. Two important points can be obtained: (1) the maximum stresses are similar, but the stress amplitudes are shown to be significantly decreased when the clamping force increases from 0 N to 8000 N, and (2) the changing trends corresponding to the clamping forces of 0 N and 2000 N were almost all the same.

The loads transferred by the bolts with different clamping forces are shown in Fig. 30(a). It is clear that (1) loads transferred by bolt-1 and bolt-4 are dominant and bear the most load, and (2) loads transferred by each bolt decrease markedly when the clamping force increases from 0 N to 8000 N. Fig. 30(b) shows the total loads transferred by the bolts and by the frictional force for the bolted joints at different clamping forces. It is clear that as the clamping force increases, the total loads transmitted by the frictional force increases, and the total loads transmitted by the bolts decreases. The decrease in the loads transmitted by the bolts leads to a reduction in the stress amplitude at the bolt hole, which is favourable for the fatigue life improvement of the scarf plate.

4.3.2. Effects on the fatigue life

The fatigue lives of the scarf bolted joints with different clamping forces were calculated, and Fig. 31 shows the calculated fatigue life versus the clamping force. Obviously, a larger clamping force results in a longer fatigue life. For all cases, the predicted crack initiates at the contact surface of the two scarf plates on the bolt hole. The failure locations of the critical element s corresponding to the

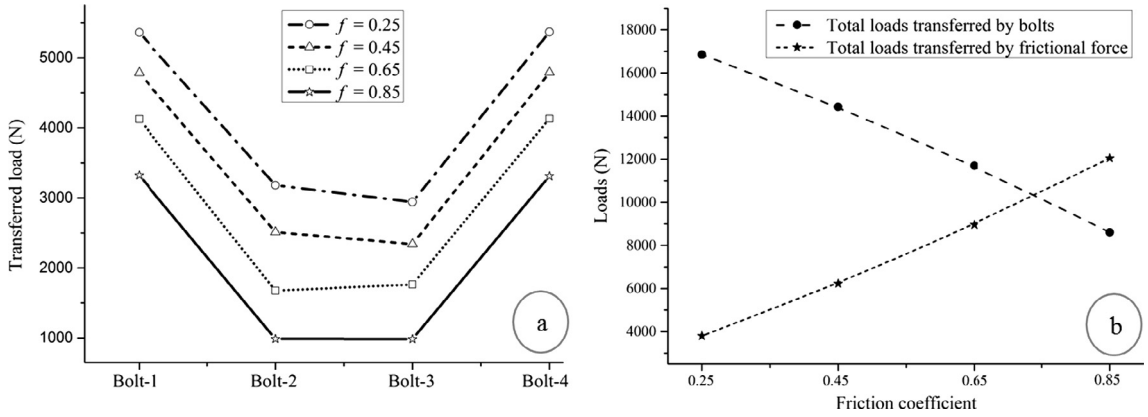

Fig. 23. (a) Effect of the friction coefficient on the load transferred by each bolt and (b) total loads transferred by the bolts and by frictional force.

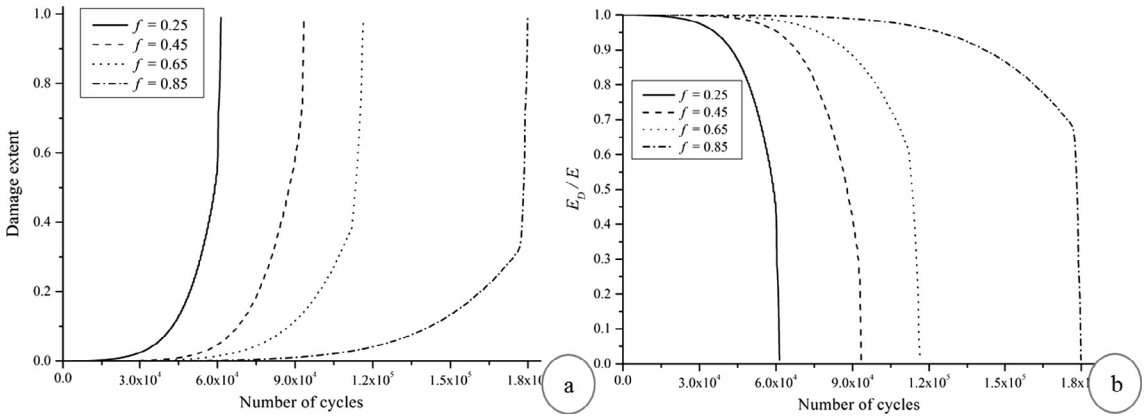

Fig. 25. (a) Damage extent versus the number of cycles with respect to different friction coefficients and (b) reduction in the equivalent Young's modulus at the critical element.

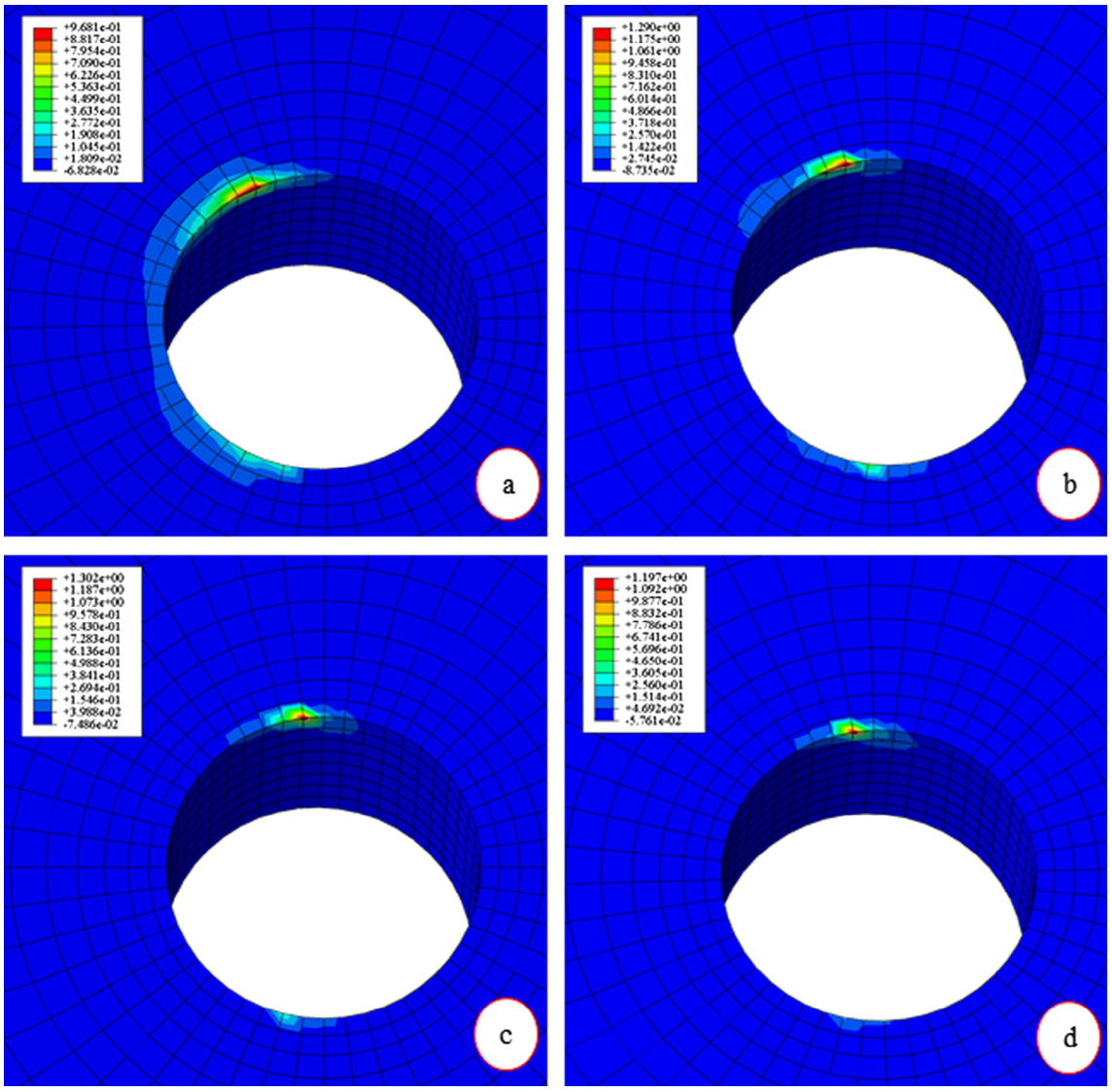

Fig. 26. Failure locations of the critical element corresponding to the different friction coefficient (a) f = 0.25, (b) f = 0.45, (c) f = 0.65 and (d) f = 0.85.

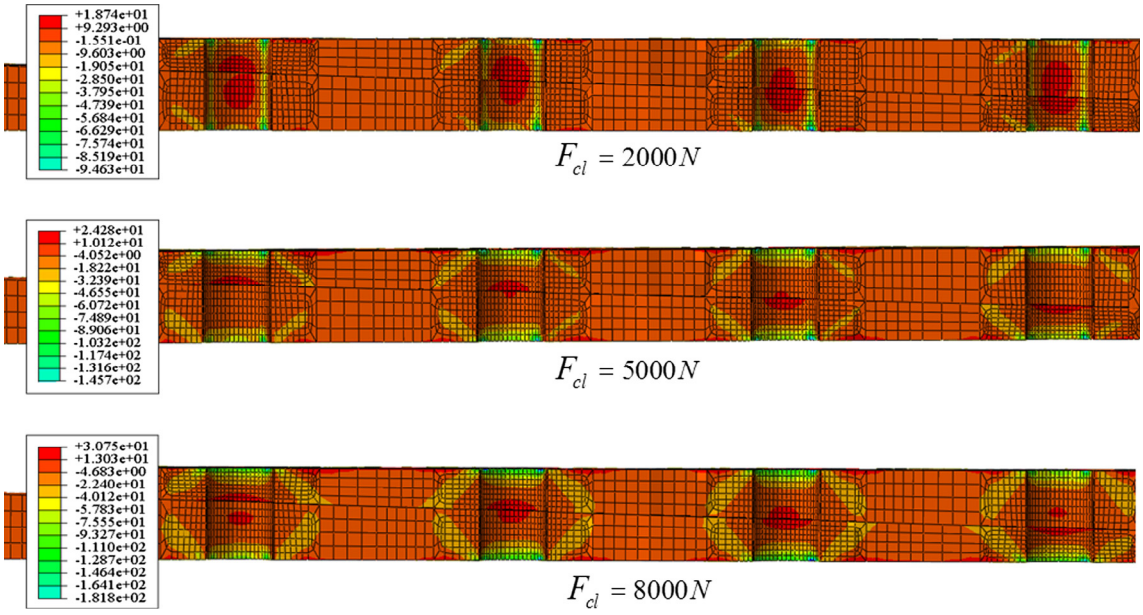

Fig. 27. Distribution of the longitudinal stress (MPa) with respect to different clamping forces.

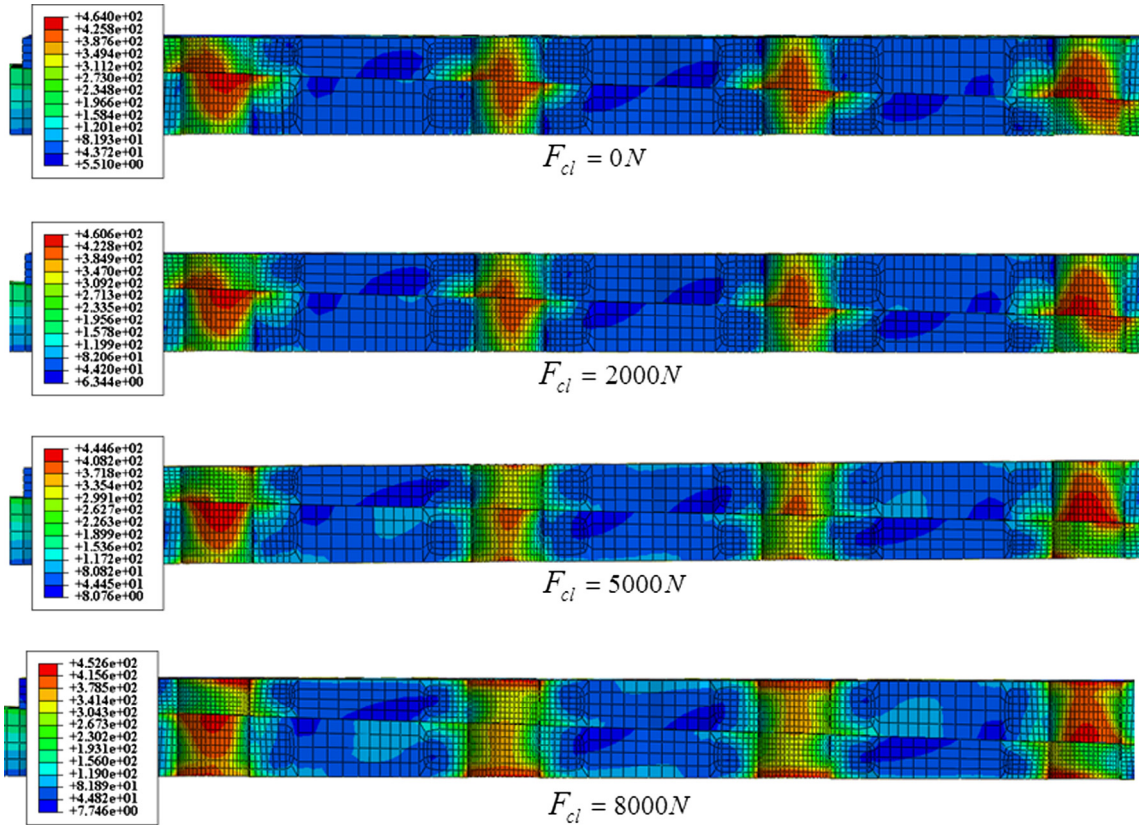

Fig. 28. Distribution of the von Mises stress (MPa) with respect to different clamping forces.

different friction coefficients are presented in Fig. 32, which shows that the failure locations of the critical elements change a little, however, which are all around the location of 90° on the bolt hole. In addition, the stress state of the critical element contains the frictional shear stress induced by the frictional force and the tensile stress induced by the cyclic loads. According to the calculated result, the tensile stress is the primary factor leading to the failure of the critical element. Thus, as the clamping force increases, although the frictional shear stress increases, the fatigue life still increases due to the tensile stress decrease.

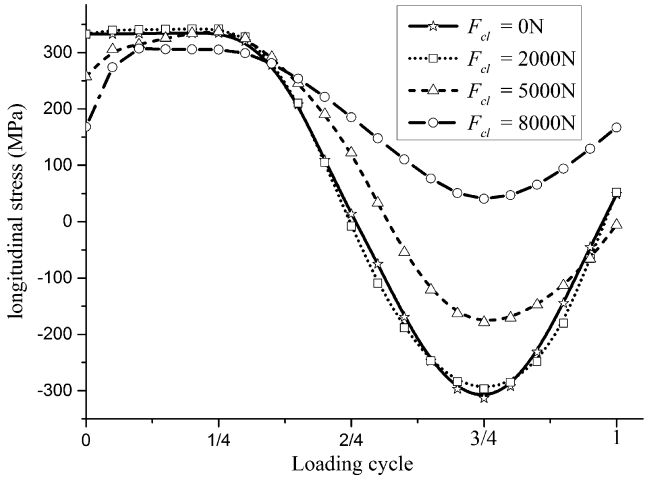

Fig. 29. Change in the longitudinal stresses (MPa) within one loading cycle with respect to different clamping forces.

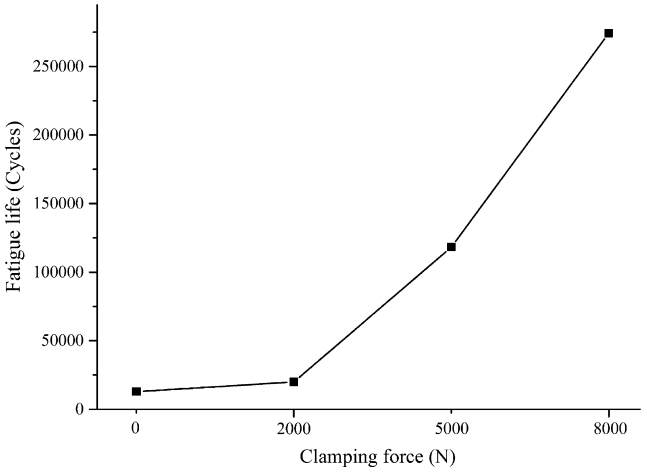

Fig. 31. Fatigue life versus the clamping force.

4.4. Sensitivity analysis of fatigue life with respect to the scarf angle, friction coefficient and clamping force

Based on the above discussion, the increases in the scarf angle, friction coefficient and clamping force all can increase the fatigue life of the joint. This section will analyse the sensitivity of the fatigue life with respect to the scarf angle, friction coefficient and clamping force. To obtain the normalized sensitivity factors, the fatigue lives of the scarf bolted joint under various conditions were calculated, and we define the sensitivity factor as the ratio between increasing multiples of the fatigue life and increasing multiples of the clamping force or friction coefficient.

First, when the scarf angle is fixed at 1.65°, the changing trends of the fatigue life along with the clamping force and friction coefficient are shown in Fig. 33. The sensitivity factors and variations in the fatigue lives along with different clamping forces and friction coefficients are listed in Table 5. The sensitivity factors were calculated according to the above definition; for example, when the clamping force increases to 8000 N, which is 4 times 2000 N, the corresponding fatigue life is approximately 13.9 times of the life at 2000 N, so the sensitivity factor of the fatigue life on the clamping force is defined as $S_{F_{cl}} = 13.9/4 \approx 3.5$; and when the friction coefficient increases to 0.85, which is approximately 3.4 times 0.25, the corresponding fatigue life is approximately 2.9 times the life of 0.25, so the sensitivity factor of the fatigue life on the friction coefficient is defined as $S_f = 2.9/3.4 \approx 0.9$. Therefore, it is obvious that the fatigue life is more sensitive to the clamping force than to the friction coefficient.

Second, when the friction coefficient is fixed at 0.65, the changing trends of the fatigue life along with the scarf angle and the clamping force are shown in Fig. 34. The sensitivity factors and the variations in the fatigue lives along with the various scarf angle and clamping forces are listed in Table 6. One can see that the fatigue life is more sensitive to the clamping force than to the scarf angle.

Third, when the clamping force is fixed at 5000 N, the changing trends of the fatigue life along with the friction coefficient and the scarf angle are shown in Fig. 35. The sensitivity factors and variations in the fatigue lives with various friction coefficients and scarf angles are listed in Table 7. It is also easy to find that the fatigue life is more sensitive to the friction coefficient than to the scarf angle.

Based on the analysis above, the fatigue life is most sensitive to the clamping force, and the sensitivity of friction coefficient is larger than the scarf angle.

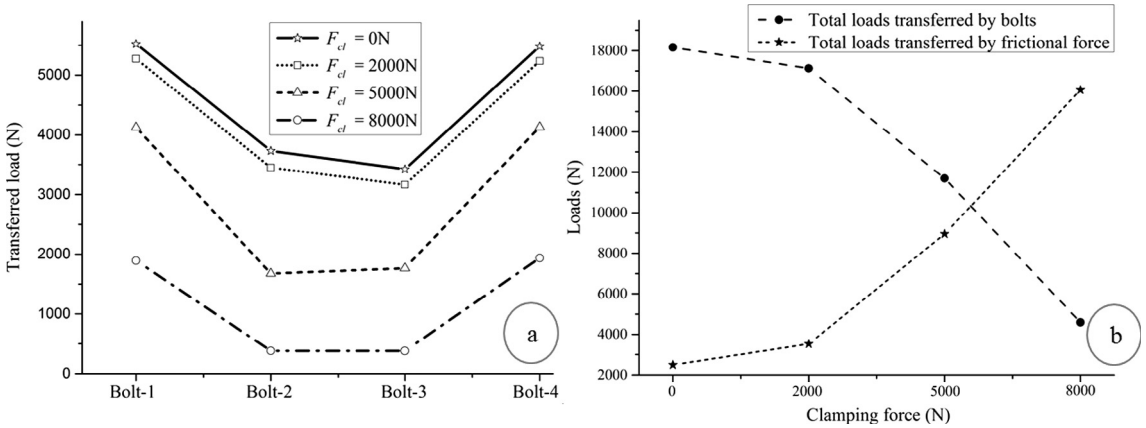

Fig. 30. (a) Effect of the clamping force on load transferred by each bolt and (b) total loads transferred by the bolts and by the frictional force.

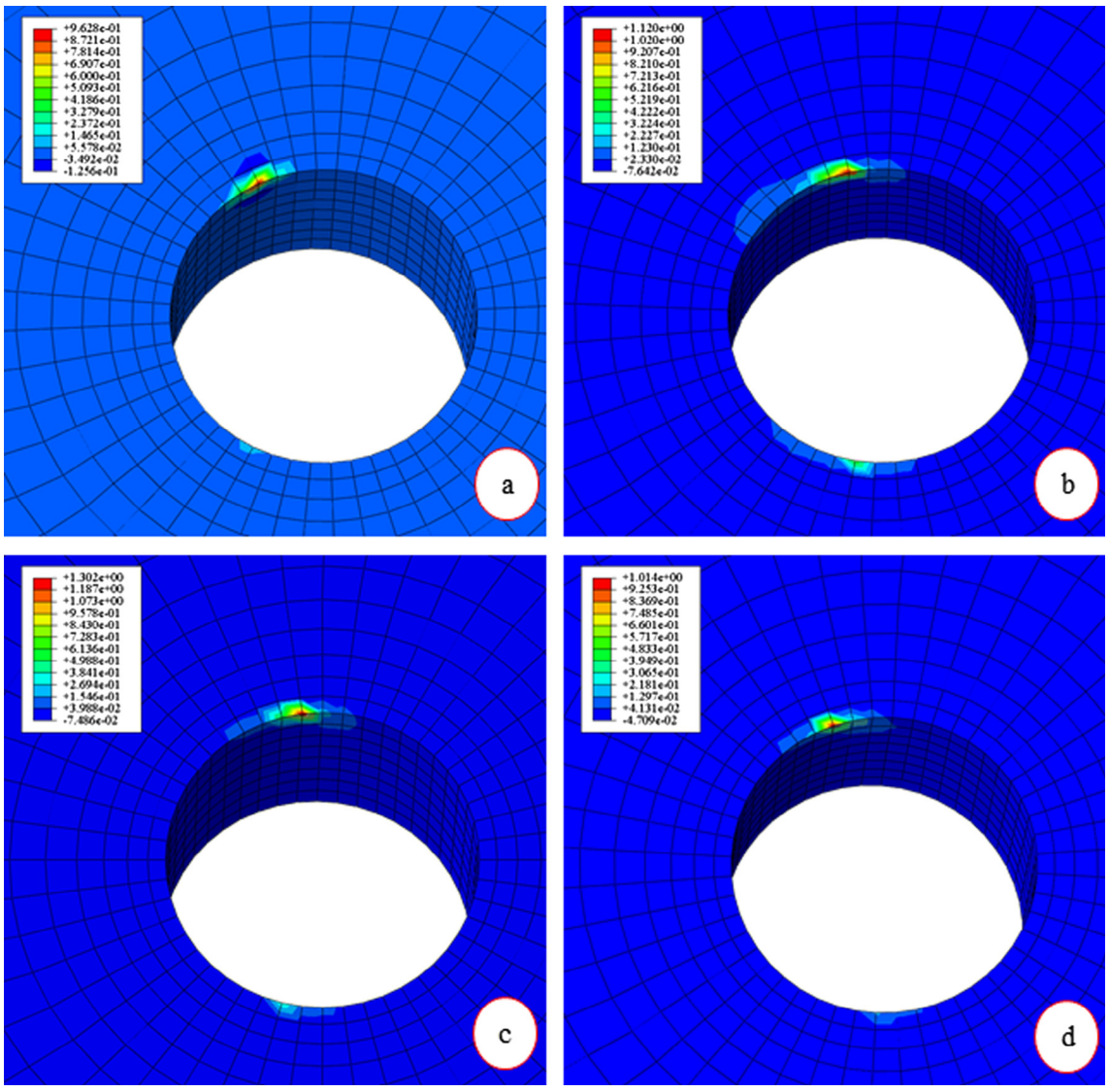

Fig. 32. Failure locations of the critical element corresponding to the different clamping force (a) F_{cl} = 0, (b) F_{cl} = 2000, (c) F_{cl} = 5000 and (d) F_{cl} = 8000.

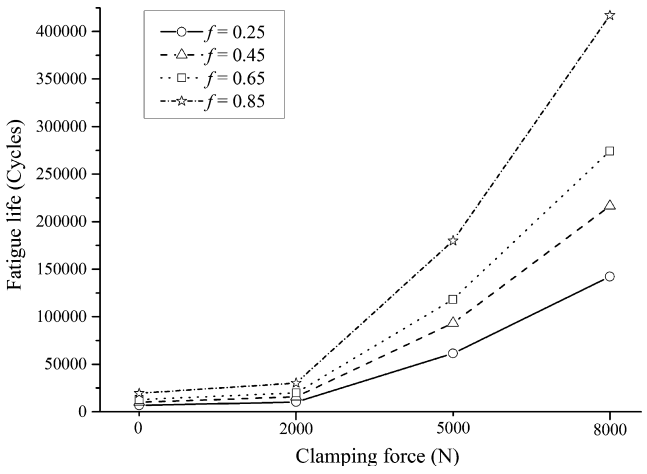

Fig. 33. Fatigue lives versus the clamping force and the friction coefficient.

Table 5
Sensitivity factor and variations of the fatigue lives along with various clamping forces and friction coefficients.

F_{cl}	F_{cl}/F_{cl2000}	$N/N_{Fcl2000}$	SF_{cl}	f	$f/f_{0.25}$	$N/N_{f0.25}$	S_f
2000 N	1.0	1.0	1	0.25	1.0	1.0	1
5000 N	2.5	6.0	2.4	0.45	1.8	1.5	0.8
8000 N	4.0	13.9	3.5	0.65	2.6	1.9	0.7
				0.85	3.4	2.9	0.9

5. Conclusions

A continuum damage mechanics-based method for the fatigue life prediction of a scarf bolted joint made of 2024-T351 aluminium alloy was proposed and validated by conducting the corresponding fatigue experiments of the components. Some of the key findings are as follows:

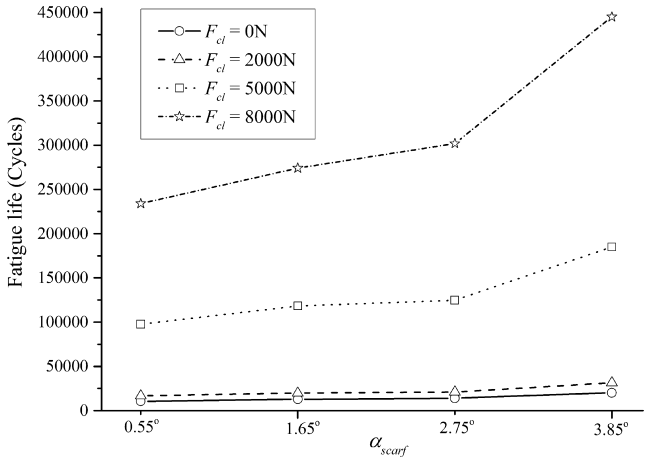

Fig. 34. Fatigue lives versus the scarf angle and the clamping force.

Table 6
Sensitivity factor and variations in the fatigue lives along with various scarf angles and clamping forces.

α_{scarf}	$\alpha_{scarf}/\alpha_{scarf0.55°}$	$N/N_{\alpha_{scarf0.55°}}$	S_{scarf}	F_{cl}	F_{cl}/F_{cl2000}	$N/N_{Fcl2000}$	S_{Fcl}
0.55°	1.0	1.0	1	2000 N	1.0	1.0	1
1.65°	3.0	1.2	0.4	5000 N	2.5	6.0	2.4
2.75°	5.0	1.3	0.3	8000 N	4.0	13.9	3.5
3.85°	7.0	1.9	0.3				

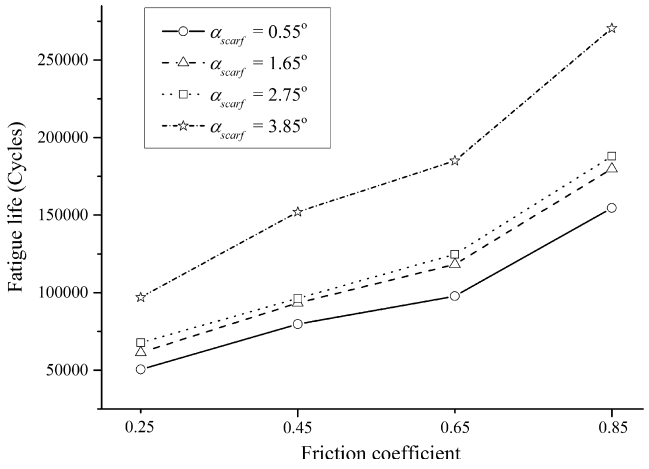

Fig. 35. Fatigue lives versus the friction coefficient and scarf angle.

Table 7
Sensitivity factor and variations of the fatigue lives along with different friction coefficients and scarf angles.

f	$f/f_{0.25}$	$N/N_{f0.25}$	S_f	α_{scarf}	$\alpha_{scarf}/\alpha_{scarf0.55°}$	$N/N_{\alpha_{scarf0.55°}}$	S_{scarf}
0.25	1.0	1.0	1	0.55°	1.0	1.0	1
0.45	1.8	1.5	0.8	1.65°	3.0	1.2	0.4
0.65	2.6	1.9	0.7	2.75°	5.0	1.3	0.3
0.85	3.4	2.9	0.9	3.85°	7.0	1.9	0.3

(1) The damage-coupled elastic-plastic constitutive equations and fatigue damage evolution equations are derived to represent the fatigue damage behaviour of the material and then implemented by user material subroutine (UMAT) in ABAQUS.

(2) The fatigue life and crack initiation site of the scarf bolted joint are predicted and are in accordance with the experimental fatigue results of the component.

(3) The scarf angle plays an important role on averaging the load transferred by the bolts and changing the stress evolution around the bolt hole. An increase in the scarf angle leads to a reduction in the stress amplitude and the maximum stress at the critical element, which can prolong the fatigue life.

(4) The friction coefficient between the scarf plates and the clamping force have similar effects on the fatigue life improvement of scarf bolted joints, and both of these factors can reduce the stress amplitude of the critical element.

(5) A sensitivity analysis of the fatigue life with respect to the scarf angle, the friction coefficient and the clamping force was performed. The calculated results show that the fatigue life is most sensitive to the clamping force, and the sensitivity of friction coefficient is greater than the scarf angle.

References

[1] Park CY, Grandt AF. Effect of load transfer on the cracking behavior at a countersunk fastener hole. Int J Fatigue 2007;29(1):146–57.
[2] Liu J, Xu HL, Zhai HB, et al. Effect of detail design on fatigue performance of fastener hole. Mater Des 2010;31(2):976–80.
[3] Fu Y, Ge E, Su H, et al. Cold expansion technology of connection holes in aircraft structures: a review and prospect. Chin J Aeronaut 2015;28(4):961–73.
[4] Ireman T, Ranvik T, Eriksson I. On damage development in mechanically fastened composite laminates. Compos Struct 2000;49(2):151–71.
[5] Chakherlou TN, Abazadeh B, Vogwell J. The effect of bolt clamping force on the fracture strength and the stress intensity factor of a plate containing a fastener hole with edge cracks. Eng Fail Anal 2009;16(1):242–53.
[6] Urban MR. Analysis of the fatigue life of riveted sheet metal helicopter airframe joints. Int J Fatigue 2003;25(9):1013–26.
[7] Samaei M, Zehsaz M, Chakherlou TN. Experimental and numerical study of fatigue crack growth of aluminum alloy 2024-T3 single lap simple bolted and hybrid (adhesive/bolted) joints. Eng Fail Anal 2016;59:253–68.
[8] Ralph WC, Johnson WS, Toivonen P, et al. Effect of various aircraft production drilling procedures on hole quality. Int J Fatigue 2006;28(8):943–50.
[9] Liu J, Yue ZF, Liu YS. Surface finish of open holes on fatigue life. Theoret Appl Fract Mech 2007;47(1):35–45.
[10] Chakherlou TN, Mirzajanzadeh M, Abazadeh B, et al. An investigation about interference fit effect on improving fatigue life of a holed single plate in joints. Eur J Mech-A/Solids 2010;29(4):675–82.
[11] Chakherlou TN, Razavi MJ, Aghdam AB, et al. An experimental investigation of the bolt clamping force and friction effect on the fatigue behavior of aluminum alloy 2024-T3 double shear lap joint. Mater Des 2011;32(8):4641–9.
[12] Lacarac V, Smith DJ, Pavier MJ, et al. Fatigue crack growth from plain and cold expanded holes in aluminium alloys. Int J Fatigue 2000;22(3):189–203.
[13] Sun Y, Voyiadjis GZ, Hu W, et al. Fatigue and fretting fatigue life prediction of double-lap bolted joints using continuum damage mechanics-based approach. Int J Damage Mech 2017;1(26):162–88.
[14] Sun Y, Hu W, Shen F, et al. Numerical simulations of the fatigue damage evolution at a fastener hole treated by cold expansion or with interference fit pin. Int J Mech Sci 2016;107:188–200.
[15] Yuan X, Yue ZF, Yan WZ, et al. Experimental and analytical investigation of fatigue and fracture behaviors for scarfed lap riveted joints with different lap angle. Eng Fail Anal 2013;33:505–16.
[16] Socie D. Fatigue-life prediction using local stress-strain concepts. Exp Mech 1977;17(2):50–6.
[17] Seshadri R. The generalized local stress strain (GLOSS) analysis—theory and applications. J Pressure Vessel Technol 1991;113(2):219–27.
[18] Jarfall L. Optimum design of joints: the stress severity factor concept. Aircraft Fatigue: Des Operat Econ Asp 1972:49–63.
[19] Ocampo J, Millwater H, Singh G, et al. Development of a probabilistic linear damage methodology for small aircraft. J Aircraft 2011;48(6):2090–106.
[20] Smith KN, Topper TH, Watson P. A stress-strain function for the fatigue of metals (atress-strain function for metal fatigue including mean stress effect). J Mater 1970;5:767–78.
[21] Chakherlou TN, Mirzajanzadeh M, Vogwell J, et al. Investigation of the fatigue life and crack growth in torque tightened bolted joints. Aerosp Sci Technol 2011;15(4):304–13.
[22] Lemaitre J, Lippmann H. A course on damage mechanics. Berlin: Springer; 1996.
[23] Lemaitre J, Desmorat R. Engineering damage mechanics: ductile, creep, fatigue and brittle failures. Springer; 2005.
[24] Naderi M, Hoseini SH, Khonsari MM. Probabilistic simulation of fatigue damage and life scatter of metallic components. Int J Plast 2013;43:101–15.

[25] Van Do VN, Lee CH, Chang KH. High cycle fatigue analysis in presence of residual stresses by using a continuum damage mechanics model. Int J Fatigue 2015;70:51–62.
[26] Zhan Z, Hu W, Zhang M, et al. The fatigue life prediction for structure with surface scratch considering cutting residual stress, initial plasticity damage and fatigue damage. Int J Fatigue 2015;74:173–82.
[27] Lemaitre J, Chaboche J-L. Mechanics of solid materials. Cambridge University Press; 1994.
[28] Chaboche JL. On some modifications of kinematic hardening to improve the description of ratchetting effects. Int J Plast 1991;7(7):661–78.
[29] Lemaitre J, Chaboche JL. Mechanics of solid materials. Cambridge: Cambridge University Press; 1990.
[30] Kang G, Liu Y, Ding J, et al. Uniaxial ratcheting and fatigue failure of tempered 42CrMo steel: damage evolution and damage-coupled visco-plastic constitutive model. Int J Plast 2009;25(5):838–60.
[31] Chaboche JL, Lesne PM. A non-linear continuous fatigue damage model. Fatigue Fract Eng Mater Struct 1988;11(1):1–17.
[32] Marmi AK, Habraken AM, Duchene L. Multiaxial fatigue damage modelling at macro scale of Ti–6Al–4V alloy. Int J Fatigue 2009;31(11):2031–40.
[33] Shen F, Hu W, Meng Q. A non-local approach based on the hypothesis of damage dissipation potential equivalence to the effect of stress gradient in fretting fatigue. Int J Fatigue 2016;90:125–38.
[34] Shen F, Hu W, Voyiadjis GZ, et al. Effects of fatigue damage and wear on fretting fatigue under partial slip condition. Wear 2015;338:394–405.
[35] Zhan ZX, Hu WP, Meng QC, et al. Continuum damage mechanics-based approach to the fatigue life prediction for 7050-T7451 aluminum alloy with impact pit. Int J Damage Mech 2016;25(7):943–66.
[36] Military Handbook – MIL-HDBK-5H: Metallic materials and elements for aerospace vehicle structures.US Department of Defense; 1998.
[37] Wu XR. Handbook of mechanical properties of aircraft structural metals. Beijing: Aviation Industry Press; 1998.
[38] Ferjaoui A, Yue T, Wahab MA, et al. Prediction of fretting fatigue crack initiation in double lap bolted joint using Continuum Damage Mechanics. Int J Fatigue 2015;73:66–76.
[39] Shigley JE, Mischke CR, Budynas RG. Mechanical engineering design. 7th ed. McGraw-Hill; 2004. p. 422–4.
[40] Klebanov Boris M, Barlam David M, Nystrom Frederic E. Machine elements: life and design. CRC Press; 2007.
[41] Zhan Z, Hu W, Shen F, et al. Fatigue life calculation for a specimen with an impact pit considering impact damage, residual stress relaxation and elastic-plastic fatigue damage. Int J Fatigue 2017;96:208–23.
[42] Zhan Z, Hu W, Li B, et al. Continuum damage mechanics combined with the extended finite element method for the total life prediction of a metallic component. Int J Mech Sci 2017;124:48–58.
[43] Zhang T, McHugh PE, Leen SB. Finite element implementation of multiaxial continuum damage mechanics for plain and fretting fatigue. Int J Fatigue 2012;44:260–72.
[44] McColl IR, Ding J, Leen SB. Finite element simulation and experimental validation of fretting wear. Wear 2004;256(11):1114–27.
[45] Jiménez-Peña C, Talemi RH, Rossi B, et al. Investigations on the fretting fatigue failure mechanism of bolted joints in high strength steel subjected to different levels of pre-tension. Tribol Int 2017;108:128–40.
[46] De Pauw J, De Waele W, Hojjati-Talemi R, et al. On the use of digital image correlation for slip measurement during coupon scale fretting fatigue experiments. Int J Solids Struct 2014;51(18):3058–66.
[47] Hojjati-Talemi R, Wahab MA, De Pauw J, et al. Prediction of fretting fatigue crack initiation and propagation lifetime for cylindrical contact configuration. Tribol Int 2014;76:73–91.